AD-A161 742 WIND DRIVEN OCEAN MODELING AND OCEAN MODEL DEVELOPMENT 1/1
(U) JAYCOR ALEXANDRIA VA A WALLCRAFT ET AL. OCT 85
J665-85-006/6251 N00014-83-C-0464

UNCLASSIFIED F/G 8/3 NL

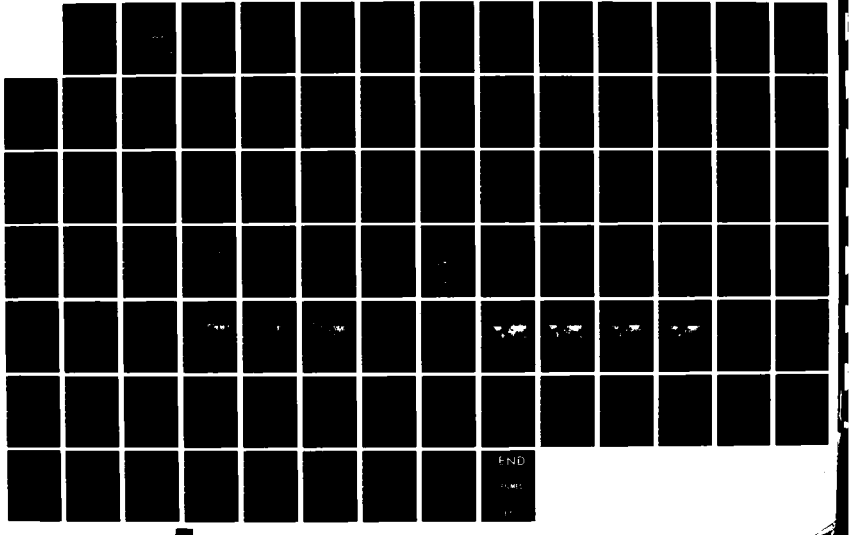

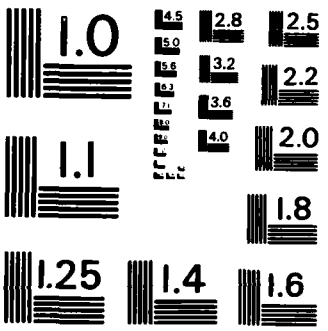

MICROCOPY RESOLUTION TEST CHART

NATIONAL BUREAU OF STANDARDS - 1963 - A

WIND DRIVEN OCEAN MODELING AND OCEAN MODEL DEVELOPMENT

FINAL REPORT

JAYCOR

205 South Whiting Street
Alexandria, Virginia 22304

WIND DRIVEN OCEAN MODELING
AND
OCEAN MODEL DEVELOPMENT

FINAL REPORT

October 1985

Submitted to:

Naval Ocean Research and Development Activity
NSTL Station, Mississippi 39529

Contract No. N00014-83-C-0464

Submitted by:

JAYCOR
205 South Whiting Street
Alexandria, Virginia 22304

Unclassified

SECURITY CLASSIFICATION OF THIS PAGE (When Data Entered)

REPORT DOCUMENTATION PAGE	READ INSTRUCTIONS BEFORE COMPLETING FORM
1. REPORT NUMBER	2. GOVT ACCESSION NO. AD-A161742	3. RECIPIENT'S CATALOG NUMBER
4. TITLE and Subtitle: WIND DRIVEN OCEAN MODELING AND OCEAN MODEL DEVELOPMENT	5. TYPE OF REPORT & PERIOD COVERED: Final Report 5/28/85-5/27/86
	6. PERFORMING ORG. REPORT NUMBER: J665-85-006/6251
7. AUTHOR(s): Alan Wallcraft, Tamara Townsend, Darren Grant	8. CONTRACT OR GRANT NUMBER(s): N00014-83-C-0464
9. PERFORMING ORGANIZATION NAME AND ADDRESS: JAYCOR, 205 So. Whiting St., Alexandria, VA 22304	10. PROGRAM ELEMENT, PROJECT, TASK AREA & WORK UNIT NUMBERS: A014
11. CONTROLLING OFFICE NAME AND ADDRESS: Naval Ocean Research and Development Activity	12. REPORT DATE: Oct. 1985 13. NUMBER OF PAGES: 85
14. MONITORING AGENCY NAME & ADDRESS(if different from Controlling Office): same as 11	15. SECURITY CLASS. (of this report): unclassified 15a. DECLASSIFICATION/DOWNGRADING SCHEDULE: N/A

16. DISTRIBUTION STATEMENT (of this Report)

1 copy - Receiving Officer, Bldg. 2105, marked for Code 332
1 copy - Scientific Officer - Code N68462
1 copy - Administrative Contracting Officer - Code N68462
1 copy - Director, Naval Research Lab, Attn: Code 2627 N00173
20 copies- Naval Ocean Research & Development Activity, Code 325-

17. DISTRIBUTION STATEMENT (of the abstract entered in Block 20, if different from Report) N68462

Same as block 16

18. SUPPLEMENTARY NOTES

None

19. KEY WORDS (Continue on reverse side if necessary and identify by block number)

Gulf of Mexico, Loop Current, ocean modeling, numerical model, Helmholtz solver, multigrid method, wind stresses, multilinear regression.

20. ABSTRACT (Continue on reverse side if necessary and identify by block number)

Numerical simulations were performed with a 0.2 deg, ~~degree,~~ two layer, free surface, primitive equation, ocean circulation model of the Gulf of Mexico with a realistic bottom topography and coastline. As in previous simulations, with idealized bottom topography and coastline, realistic Loop Current behavior could be obtained without wind forcing and with constant inflow through the Yucatan Straits. However, simulations with both wind and port

DD FORM 1 JAN 73 1473 EDITION OF 1 NOV 65 IS OBSOLETE S/N 0102-LF-014-6601

Unclassified

SECURITY CLASSIFICATION OF THIS PAGE (When Data Ent

20. Abstract (continued)

forcing showed significantly more variation than those with port forcing alone.

A similar two layer model, ~~has been~~ set up for a North Atlantic region, from 20N, 82W to 48N, 30W, on a 0.25 by 0.2 degree grid.

A "~~Black Box~~" multigrid package ~~has been~~ prepared for solving finite difference Helmholtz's equations with staggered grid Neumann boundary conditions in nonrectangular regions. In semi-implicit free surface primitive equation ocean models, it is competitive with other powerful iterative methods but slower than the direct Capacitance Matrix Technique.

Several wind stress data sets ~~have been~~ prepared for use in ocean models, based on global analysis products from FNOC and NMC, regional analysis products from FNOC, and ship observations. These data sets have been used to drive ocean circulation models of the World Ocean, the Indian Ocean, the North Atlantic, and the Western Mediterranean Sea.

The capabilities of a statistical model to nowcast subsurface pressure information from free surface data obtained by a hypothetically perfectly accurate altimeter was explored. Pointwise linear regression of upper to lower layer pressure did not lead to successful lower layer predictions. Pointwise multilinear regression was more successful, particularly in predominantly barotropic regions. However it did not do well in regions of very strong baroclinic instability. Statistical prediction appears to be a promising technique for initializing dynamical ocean circulation prediction models.

TABLE OF CONTENTS

I. GULF OF MEXICO MODELING

This is a continuation of modeling in the Gulf of Mexico previously performed by NORDA (Hurlburt and Thompson, 1980 and 1982). The same two layer, primitive equation, free surface, hydrodynamic model with topography confined to the lowest layer is used as before, but with the addition of 'realistic' (rather than idealized) coastline geometry and bottom topography. The ocean model contains many innovative features and the reader is referred to its detailed discussion in Hurlburt and Thompson (1980). In particular, Section 2 (pp 1613-1614) gives the model equations and Appendix B (pp 1647-1650) describes the numerical design of the model. Since that time the capability to handle general basin geometry has been added but this does not affect the description in any major way. Wind forcing is treated identically to interfacial and bottom stress terms, i.e., wind stress appears directly as an additive term in the momentum equation [see p 1614 of Hurlburt and Thompson (1980)].

In terms of 'realism' Experiment 9 was the most successful port driven Gulf of Mexico numerical simulation produced under this contract. The model was driven from rest to statistical equilibrium solely by a steady inflow through the Yucatan Straits which was compensated by outflow through the Florida Straits. The model parameters were:

- upper/lower layer inflow transport = 26/4 Sv,
- wind stress = 0,
- horizontal eddy viscosity, A = 300 m^2/sec,
- grid spacing = 25 by 25 km,
- reference layer thicknesses, H1 = 200m and H2=3400m,
- minimum depth of bottom topography = 500m,
- beta, df/dy = $2*10^{-11}$ m^{-1} sec^{-1},
- Coriolis parameter at the southern boundary, f = 5×10^{-5} sec^{-1},

- gravitational acceleration, g = 9.8 m/sec^2,
- reduced gravity, g' = .03(H1+H2)/H2 m/sec^2,
- interfacial stress = 0,
- coefficient of quadratic bottom stress = .002, and
- time step = 1 hour.

Figure 1 compares 'instantaneous' upper ocean flow patterns just before an eddy is shed by the Loop current (a) from the numerical model and (b) from observations by Leipper (1970). The ability of the model to simulate observed features is clearly demonstrated by this comparison, which is remarkable given the simplicity of the model forcing. However some discrepancies remain, for example the eddy has not penetrated as far into the Gulf and is more intense than that shown in the observations. Waves can be seen moving around the wall of the Loop Current in both the model and the observations, but in the model they are at the limit of resolution and therefore unrealistically large. Moreover in the Gulf the waves are more pronounced on the eastern wall of the Loop and can form strong cold intrusions that may contribute to the eddy shedding process (Vukovitch and Maul, 1984). As shed eddies propagate westward (Figure 2a) the model spontaneously develops a counter rotating vortex pair (Figure 2b), a structure repeatedly observed in the Western Gulf (Figure 3). The roles of the wind and the Loop current eddies in the formation of this structure have been a matter of some controversy (Merrell and Morrison, 1981). Although wind forcing was not present in this simulation a major role for winds has not yet been ruled out. After spin-up the experiment sheds an eddy once every 390 days and the eddy shedding cycles are very similar.

Experiment 28 is identical to Experiment 9, except for the grid spacing (20 by 22, rather than 25 by 25 Km) and the Coriolis parameter (4.5×10^{-5}, rather than 5×10^{-5} sec^{-1}). It gives very similar results. Experiment 31 uses the same

model parameters as Experiment 28, but has no port forcing being driven instead by seasonal climatological winds based on ship observations (Elliot, 1879). Linear interpolation in time was used between the seasonal fields to produce the wind stress at each time step. The experiment reaches an annual steady state cycle, winds and associated circulations for each season are shown in Figures 4 to 7 (note the contour interval is 12.5 m rather than the more usual 25 m). Upwelling in the south west Gulf in the fall and winter, and a persistent anticyclonic 'Texas' coastal current are the major features of the simulation.

Experiment 34 combines the wind and port forcings of Experiments 28 and 31. Model parameters were:

- upper/lower layer inflow transport = 26/4 Sv,
- wind stress from seasonal climatology based on ship observations,
- horizontal eddy viscosity, A = 300 m^2/sec,
- grid spacing = 20 by 22 km (0.2 by 0.2 degrees),
- reference layer thicknesses, H1 = 200m and H2=3300m,
- minimum depth of bottom topography = 500m,
- beta, $df/dy = 2*10^{-11}\ m^{-1}\ sec^{-1}$,
- Coriolis parameter at the southern boundary, $f = 4.5 \times 10^{-5}\ sec^{-1}$,
- gravitational acceleration, $g = 9.8\ m/sec^2$,
- reduced gravity, $g' = .03(H1+H2)/H2\ m/sec^2$,
- interfacial stress = 0,
- coefficient of quadratic bottom stress = .002, and
- time step = 1.5 hours.

Seasonal climatological winds obviously cannot represent most of the wind variability and persistence. Even so the addition of wind forcing increases the variability of the Loop Current system, including the eddy shedding period and eddy path. For example Figure 8 compares 360 model days from Experiments 28 and 34 (which

are identical except that Experiment 28 has no wind forcing). From these snapshots, taken every 90 days, there is little difference between the two experiments. But if Experiment 34 is sampled every 20 days, as in Figure 9, it is apparent that two eddies were shed in the space of about one year. Figure 9 also shows that the circulation pattern in the Western Gulf can change very rapidly at times. Figure 10 shows the mean interface deviation and its variability for experiments with wind forcing only, port forcing only and with wind plus port forcing. This demonstrates that even in the mean the interaction of wind and port forcing is not linear, i.e., the mean of the dual forcing experiment is not the sum of the other two means. The variability is increased in the dual forcing case, particularly in the central and western Gulf.

More recent work has largely superseded the experiments described above. In particular a ratio of 20/10 Sv for upper/lower layer transport is now preferred over the 26/4 Sv used here, and wind driven experiments have been performed with wind data based on the Navy's twelve hourly surface pressure analysis from 1967 to 1982 (Wallcraft, 1985). The differences between the seasonal means from the 12 hourly data and the ship observation data is significant, particularly in the south west Gulf (Rhodes, Thompson and Wallcraft, 1985). Therefore emphasis should not be placed on the details of the wind driven experiments described above.

II. NORTH ATLANTIC MODELING.

The aim of this modeling effort was to set up a finite depth ocean model of a large ocean basin. Detailed modeling experiments were not performed. The major difference between the small basin models (of the Gulf of Mexico, for example) and a North Atlantic model is that the beta-plane approximation no longer applies so spherical coordinates must be used. Explicit reduced gravity versions of large basin models already existed (NORDA's World Ocean Model, for example), and the major difficulty in producing the finite depth model was the development of the correct Helmholtz solver for the spherical semi-implicit equations. At the same time the two-layer finite depth model was generalized to n-layers, for both the beta-plane and for spherical coordinates. This involved the replacement of precalculated constants for transformation into modal space, with numerically derived values.

The model region is from 20N, 82W to 48N, 30W and all boundaries are closed with free slip conditions being applied to the east and south boundaries. The grid spacing is 0.25 by 0.2 degrees, i.e., delta-x varies from 26 km (at 20N) to 19 km (at 48N) and delta-y is about 22 km. This is the smallest closed region that is viable for studying the Gulf Stream. A larger region (and finer grid) would be preferable, but would require a faster machine with more main memory than the CRAY X-MP 1200 used for these experiments.

Figure 11 shows the coastline and bottom topography used by the model. The topography is from SYNBAPS, the minimum depth is 1000 m and it has been smoothed twice by a nine point real smoother. Figure 12 is a plot of interface deviation from the seventh year of an experiment forced, from rest, with monthly climatological winds. A meandering Gulf Stream has been spun up by this simulation, however its

separation point from the coast and penetration distance are not 'realistic'. The simulation was only performed to check out the ocean model, it is expected that a full scale modeling effort in the North Atlantic will be started by NORDA in the near future to take this work further.

III. MULTIGRID SOLVER.

Multigrid techniques are a relatively new set of methods for greatly accelerating the convergence of the classical iterative techniques for the solution of elliptic partial differential equations (Brandt, 1982). Multigrid iteration involves a sequence of grids, each with about four times as many nodes, or computational points, as its coarser predecessor. On each grid (except the coarsest), high frequency error components are reduced by a classical iterative method and low frequency errors by extrapolation from the solution of a related problem on the next coarsest grid. The methods great speed is based on the fact that many iterative procedures reduce high frequency errors very rapidly, and also on the relative cheapness of solutions on coarse grids.

In NORDA's layered semi-implicit primitive equation free surface ocean circulation models the solution of several finite difference Helmholtz's equations are required to relatively high accuracy (about 5 or 6 places of decimals) each time-step (one per layer). These equations have staggered grid Neumann boundary conditions, and are over the general irregular regions formed by ocean basins (not over a rectangle, which would be computationally simpler). Classical multigrid methods could be applied to such problems, but the irregular geometry and Neumann boundary conditions give rise to bookkeeping and algorithmic difficulties. An alternative is to use a "black box" multigrid method (Dendy, 1982), which acts on the general finite difference form of the equations and makes minimal assumptions about the underlying continuum problem.

A public domain black box multigrid solver (Dendy, 1982) has been modified for NORDA's ocean models. The original code was for general coefficient finite difference 9-point elliptic equations in a rectangle with discontinuous

coefficients. This code applies equally to five-point Helmholtz's equation with Neumann boundary conditions over a nonrectangular region, since the irregular boundary is equivalent to a discontinuity. Black box multigrid always uses a nine-point operator on the coarser grids, even when the finest operator is five-point. On the other hand the irregular boundary needs no special coding on the coarse grids. Modifications to the original code include:

a) Uses red-black (four color for nine-point equations) pointwise Gauss Seidel as the underlying iterative scheme, because it is highly vectorizable.
b) Modified finest grid code to handle the required Helmholtz's equations only. This saves both storage and time over the general version.
c) Fully vectorized the solution phase of the solver, the preprocessing stage has not been vectorized since it is only called at the beginning of a model run.

Total storage requirements are 3.3 meshes per equation for constants, and 2 workspace arrays. Table 1 gives times, on a CRAY X-MP 1200, for the multigrid code and for a fast direct rectangular Helmholtz solver (based on a FFT) over various sized rectangles. The multigrid code is equally as fast on nonrectangular regions. The FFT based solver can be extended to general regions via the Capacitance Matrix Technique (Buzbee, et. al., 1980) but solve times are two to three times as long and a large amount of storage can be required.

TABLE 1 - GRID SIZE vs. SOLVE TIME and TIME PER NODE, FOR TWO HELMHOLTZ SOLVERS ON A CRAY X-MP 1200

GRID SIZE	SOLVE TIME (sec) and (TIME PER NODE (micro-sec))		
	MULTI-GRID 1	MULTI-GRID 2	FACR(1)
13 x 13	.0027 (16.2)	.0017 (9.8)	.0006 (3.7)
25 x 25	.0089 (9.5)	.0031 (4.9)	.0010 (1.7)
49 x 49	.0176 (7.3)	.0079 (3.3)	.0024 (1.0)
97 x 97	.0634 (6.7)	.0256 (2.7)	.0066 (0.7)

Notes:

1) All multigrid times are averages to reduce the original relative error by 10^{-6}. This is probably a worse case for ocean models, where typical required error reduction is about 10^{-3}.
2) Multigrid-1 is a case with a small Helmholtz parameter, and multigrid-2 a case with a large parameter. These correspond to external and internal gravity modes respectively in the ocean model.
3) Multigrid-1 takes about 5 to 7 major iterations, Multigrid-2 about 2 to 3 iterations for 10^{-6} improvement in accuracy.
4) FACR(1) is a fast direct solver that only works for rectangles, minimum direct solve time over irregular regions is 2 to 3 times longer.

IV. BOTTOM TOPOGRAPHIES

The global Synthetic Bathymetric Profiling System (SYNBAPS) data set is uniquely suited to the generation of ocean model bottom topographies. It differs from the earlier Northern Hemisphere version in covering 99 percent of the world ocean, and in being organized on a geographic grid (five minute grid spacing) rather than on a meridional parts grid (Van Wyckhouse, 1973).

A VAX/VMS specific FORTRAN 77 package has been developed that extracts bottom topography for NORDA's ocean models from the SYNBAPS data set. The capability to set the coastline at any desired depth below sea level, and to cut off the continental shelf at any depth is included. The coastline capability is required because setting the coast at, say, 100 m below sea level might be appropriate in some cases (particularly for reduced gravity models). The continental shelf cut off is required because bottom topography must be constrained to the lowest layer in layered models, typically the shallowest topography might be at 500 m or more below sea level. SYNBAPS can give rise to unacceptable coastlines, in isolated areas, either because SYNBAPS has no data there or because of interpolation difficulties. Such areas must be cleaned up by hand, and as an aid to their isolation and correction, graphics display software and interactive node modification procedures have been included in the package. Nine point real smoothers are also provided, since two delta-x waves are undesirable in model bottom topographies.

Figure 13 shows the 0.1 degree Gulf of Mexico topography, as originally generated by the package from the raw SYNBAPS data. To reach this stage requires about fifteen minutes (wall clock time), from entering the package to obtaining a hardcopy of the plot. The coastline is taken as the 10 m depth contour, and all topography shallower than

500 m is set to 500 m to ensure that the topography is confined to the lowest layer of the ocean model. Note that there is no SYNBAPS data available in the rectangle bounded by (95W, 29N) and (90W, 30N), there are several regions in the world ocean where SYNBAPS has no data for small areas near the coast. This is apparently to reduce the size of the data base, since these regions can only be included if large areas over land are also present.

Figure 14 shows the 0.1 degree Gulf of Mexico topography modified for use in the ocean model. The coastline has been extensively edited, primarily to improve to look of graphical output rather than for modeling constraints (the actual model coastline is largely that shown in the previous figure). The Caribbean Sea is not part of the model region, and has therefore been set to land (although the Caribbean coastline is still shown on plots). Finally a nine point real smoother has been applied to the topography twice to remove small scale variations. Production of this version took about one day, it is of about average size (180 by 130) but has far fewer problems with islands and narrows than some other regions.

The SYNBAPS extraction package can only be accessed interactively, via a DCL command file. It provides sufficient information on the screen to allow anyone familiar with the target ocean model code to produce a topography field for a new region without difficulty. Topographies have been created for ocean models of: the World Ocean, the North Atlantic Ocean (Figure 11), the Indian Ocean, the Gulf of Mexico, and the Mediterranean Sea.

V. WIND STRESS DATA SETS.

The following wind data sets have been used to compute wind stress fields, which in turn have been or will be implemented in the World Ocean Model or other single-basin ocean models currently being developed by NORDA Code 323. In all cases, the following equations were used to compute the x- and y-components of the wind stress, τ:

$$\tau_x = \rho C_D |\vec{V}| u, \qquad \tau_y = \rho C_D |\vec{V}| v,$$

where ρ is the air density in g/cm^3, C_D is the drag coefficient, for which the value 0.002 was used, $|\vec{V}|$ is the magnitude of the wind velocity, u is the x-component of the wind velocity, and v is the y-component of the wind velocity. The exception was the Hellerman data, which was received in the form of u and v wind stress components. The spatial interpolation scheme utilized was a repeated application of a one-dimensional Bessel interpolation of the third order involving the sixteen values closest to the desired grid point.

NOGAPS

Two products of the Fleet Numerical Oceanography Center (FNOC) Naval Operational Global Atmospheric Prediction System (NOGAPS) analysis are the planetary boundary layer u- and v-components of the wind (cm/s) on a 144 by 73, 2.5° by 2.5° grid that extends from 90S to 90N and 60E to 57.5E. These wind components, available at 0000Z and 1200Z synoptic times, for the year 1983 (the first complete year available) were retrieved from FNOC's archives for use in developing the mean u- and v-components of the wind stress for each month of that year. The procedure was as follows. First, the wind stress components ($dynes/cm^2$)

at each grid point were computed. Then the monthly averages of these components were calculated. Before storing the results on tape at FNOC, the entire grid was shifted westward so that 180W formed the western edge and an additional column was added to the eastern edge of the grid, a duplicate of the column on the western edge. Thus, the grid for τ_x and τ_y now extends from 180W to 180W in the x-direction.

The monthly-mean wind stress components, derived from the NOGAPS u- and v-components of the wind, were stored on tape at FNOC in order to facilitate implementation of these fields in the World Ocean Model, which is run on the FNOC CYBER 205 vector-processing computer. One additional step before utilization by the model was transfer of the τ_x and τ_y monthly-mean fields to the CYBER 205 after spatial interpolation to the 243 by 111, 1.5° by 1.25° World Ocean Model grid. The x- and y-components of the wind stress were staggered such that the southwest corners of the τ_x and τ_y grids were at 66.25S,179.2W and 65.625S,171.25W, respectively. (There was some overlap in the x-direction). Figure 15 shows the monthly-mean wind stress curl for January, April, July, and October of 1983.

Hellerman Wind Stress Climatology

This data set consists of the climatological monthly-mean wind stress components, τ_x and τ_y, over the world ocean on a 180 by 90, 2° by 2° grid that extends from 89S to 89N and 1E to 359E. Hellerman (1967) computed these wind stress components using wind rose data and the above equations, where

$C_D = 2.43 \times 10^{-3}$ for windspeeds of at least Beaufort force 7

and

$$\rho = \begin{cases} (.0022\theta + 1.136) \times 10^{-3} & \theta > 20° \\ 1.18 \times 10^{-3} & -20° < \theta < 20° \\ (-.0028\theta + 1.124) \times 10^{-3} & \theta < 20° \end{cases}$$

These data were interpolated and shifted westward onto the 145 by 73, 2.5° by 2.5° grid used for the NOGAPS 1983 wind stress components to facilitate generation of graphics using an existing plot routine and comparison of the two data sets. The data were then interpolated to the 243 by 111, 1.5° by 1.25° World Ocean Model staggered u- and v-grids and stored on disk on the FNOC CYBER 205 for use in the World Ocean Model.

The τ_x and τ_y wind stress components were interpolated to the Indian Ocean and North Atlantic Model staggered grids in a similar manner. The Indian Ocean Model area extends from 10S to 27N and 35E to 106E and the southwest corner of the u-component grid is at 10S, 38.1E and that for the v-component grid is at 10.1S, 38E. An enlarged version of the model extends from 25S to 27N and 38E to 106E so that the lower left point on the u-component grid is at 65S, 38.1E and the same point on the v-component grid is at 65.1S, 38E. For both model regions, the u- and v-wind stress components have been stored on a 0.2° by 0.2° grid and a 0.4° by 0.4° grid. In the case of the North Atlantic Ocean, the model region extends from 20N to 48N and 82W to 30W and the wind stresses have been stored on a 209 by 136, .25° by .2° grid. The u- and v-grids are staggered such that the lower left point of the τ_x wind stress component is at 20N, 81.875W and that of the τ_y wind stress component is at 20.1N, 82W. Figure 16 is the same as Figure 15, except that it is for the Hellerman global wind stress curl.

NMC

An additional global data set is the National Meteorological Center (NMC) analysis on 2.5° by 2.5° northern and southern hemispheric grids where the 0 longitude forms the western boundary. The 1000-mb u- and v-wind components from this analysis for the period 1 July 1976 through 29 May 1982 at twice-daily intervals were received from the National Center for Atmospheric Research (NCAR) in the NMC packed data format that is described in Office Note 84 (NMC, 1979). The two hemispheric grids were merged into one 145 by 73, 2.5° by 2.5° global grid and shifted so that 180W forms the western boundary. As was done for the previously discussed data sets, the τ_x and τ_y wind stress components were computed for each analysis time. Interpolation over time (not more than three days) filled in the missing times for which the winds were not available. After interpolating, the mean wind stress components were computed for each month of each available year.

NORAPS

In addition to the NOGAPS model, FNOC has a Naval Operational Regional Atmospheric Prediction System (NORAPS) for production of numerical forecasts over limited areas of the earth. The northern hemisphere is one such area for which this system is implemented on a 63 by 63 polar stereographic grid with the North Pole at the center of the grid and a grid distance of 381.00 km at 60N. The Mediterranean Sea 63 by 63 polar stereographic grid is a subset of this grid that has been zoomed four times with no rotation. It has a grid distance of 95.25 km at 60N. It is from the Mediterranean grid that only those u- and v-wind components in the immediate vicinity of the western Mediterranean Sea are retrieved from FNOC on a twice-daily

basis and stored at NORDA. Before computing the τ_x and τ_y wind stress components, the u- and v-wind components were translated from the polar stereographic grid to a latitude-longitude grid and interpolated to the 109 by 93, 0.1° by 0.05° western Mediterranean Sea Model staggered grid, i.e., the southwest corner of the u-wind component grid is at 35.2N, 354.55E and that for the v-wind component is at 35.225N, 354.5E. The wind stress components and their monthly means were then computed for September 1984, the first complete month of data received through August 1985, the latest complete month available. Figure 17 shows the wind stress vectors and Figure 18 the wind stress curl over the NORDA western Mediterranean Model region for October 1984 and January, April and July 1985.

VI. STATISTICAL SURFACE TO SUBSURFACE DATA CONVERSION.

Hurlburt (1985) discusses the capabilities of a numerical model of ocean dynamics to forecast subsurface pressure information from altimetrically derived sea surface height data. This project, intended to complement Hurlburt's work, explores the capabilities of a statistical model to nowcast subsurface pressure information from data obtained by a hypothetically perfectly accurate model altimeter. Using height data derived solely by a numerical ocean model, this study employs a series of regression models to relate the surface information to subsurface information.

The testbed region was the Gulf of Mexico, approximated by a 1600 km by 900 km rectangular box with 20 km by 18.75 km grid resolution. The model used was the same hydrodynamic, two layer, finite depth, primitive equation ocean circulation model used in Hurlburt's work. Selected model simulations provided the "true" data for the regressions, the predictions, and the error calculations. Experiments were run using data from simulations with barotropic and/or baroclinic instability, with a short and/or a long major time scale, and with flat or large amplitude bottom topography. The two model runs chosen for detailed study were:

E1 - a nearly periodic, barotropically unstable, run with large amplitude bottom topography, and
E2 - a highly baroclinically unstable run with flat bottom topography.

Both simulations generate two pressure fields, P1 and P2, upper (surface water) and lower (deep water) pressure, respectively. Furthermore, although E1 and E2 have vastly different dynamics, each is characteristic of a major dynamical regime present in the world's oceans (but not necessarily of the actual Gulf of Mexico).

The first series of experiments used pointwise linear regressions of every P1 point from the model to the P2 point directly beneath, an approach similar to that of DeMey and Robinson (personal communication), who assumed spatial homogeneity and solved one regression equation for the entire POLYMODE region. Our results were also similar, about 70 percent spatial NRMS error for E1 and 80 percent spatial NRMS error in E2 for predictions made on independent data sets. These were clearly insufficient for successful deep water prediction.

The next series consisted of a pointwise multilinear regression of a set of synoptic P1 data to a P2 point. For computational and statistical stability the regression was done with only the statistically meaningful principal components of the P1 set chosen. Correlations were used to identify ideal choices of predictors. The tradeoff is between having sufficiently independent information in the P1 field, which often means a greater distancing of predictors, and having information sufficiently correlated with the P2 field, which often implies predictors crowded around the center of the prediction; however, reasonable but not optimal choices of predictors rarely harmed the regressions' accuracy significantly. Often a 5 point star of the P1 point directly above the P2 point being predicted and points directly north, east, south, and west of it, with a radius of 40 to 60 km, was sufficient.

This technique predicted E1 very well on an independent data set, with spatial NRMS error of about 0.2 to 0.3. Figures 19 and 20, respectively, show "real" (model derived) lower layer pressure, and predicted (statistically derived) lower layer pressure fields, at a representative time in this experiment. As in all the figures, north is at the top. All major features are accurately depicted both in strength and in location, as is

evidenced by the low spatial NRMS error for the grid. The multilinear principal components regression (MPCR) also gave good but increasingly worse results on sister experiments with greater baroclinic instability and less periodicity. In E1 the eddy viscosity, A, is 300 m^2/sec. A similar run with A = 150 gave predictions with NRMS of 0.3 to 0.5, and with A = 100, NRMS is 0.4 to 0.65. Eddy mean energetics for all experiments listed in this report can be found in Hurlburt [1985; Experiments T3A (E1), T3B, T3C, and T1 (E2)].

On E2, errors were still unacceptably high, with NRMS of 0.65 to 0.75. It was noticed, as might be expected, that predictions were acceptable in mostly barotropic subregions with little eddy activity, but were very poor otherwise, often misplacing or totally misrecognizing deep water eddies. Furthermore, one dominant structure in this region of poor skill was the major eddy in the upper layer and an associated deep water counter-rotating vortex pair.

Figures 21 and 22 show the upper layer pressure field (P1) and the lower layer pressure field (P2), respectively, for a day near the end of the fifth year of experiment E2. In Figure 21 an eddy is about to be shed from the loop current, as a previously shed eddy begins to die to the west. Note the counter rotating vortex pair in the lower layer, and the great variability in the lower layer pressure field. Figure 23 contours a prediction using a MPCR of the P1 field to the P2 field. Most of the error comes from severe inaccuracy in the western and southwestern portion of the basin, the region of high baroclinic instability and of frequent eddy activity. In the barotropic northern and northeastern region of the Gulf the results are fairly accurate.

The above considerations motivated the use of a limited Lagrangian coordinate MPCR. A square box the length of the major Loop Current eddy (about 300 km), and centered

on it was allowed to move with the eddy through a complete eddy cycle. The regression was performed relative to the box, selecting predictors in a five-point star as previously stated. In E2 on the dependent data set the NRMS in the region of the eddy is 0.4 to 0.6, implying a significant increase in skill over the Eulerian coordinate formulations. Figures 24 and 25, respectively, show the "real" and predicted lower layer pressures in the box described above at the same time in E2 as is shown in Figures 21-23. The region in Figure 24 corresponds to the box drawn in the right center of Figure 21. One can see a considerable increase in skill in the prediction, both in determining the strength and location of the large anticyclonic eddy to the south and in prediction of the corner of the eddy to the northwest.

Kindle (1985) notes the sufficiency of three or four cross altimeter tracks to accurately resolve an irregularly shaped eddy. This corresponds in our discretization to about 80 km by 65 km resolution. Subsampling the entire grid to this degree of resolution still permitted statistical predictions without a serious loss of accuracy; that is, the sparser resolution usually gave acceptable results when the finer resolution gave acceptable results. This intimates that practical usage of the statistical model given altimetrically derived data is feasible.

Although the Eulerian methods tried show only nowcast skill, not forecast skill, since the decorrelation time scale of each model was only 20 days or less, dynamical forecasts using the Eulerian MPCR computed initial P2 field have often been successful (Hurlburt, 1985; personal communication). Combining the statistical and dynamical approaches, using statistically derived information for initial fields and forecasting an optimal estimation of the P2 field from the statistically and dynamically predicted

fields, holds great promise and potential for building an operational ocean prediction scheme.

VII. REFERENCES

1. Brandt, A. 1982: "Guide to Multigrid Development" in W. Hackbusch and U. Trottenberg (eds), Multigrid Methods, Springer-Verlag.
2. Buzbee. B.L., Dorr, F.W., George, J.A. and Golub, G.H. 1971: "The Direct Solution of the Discrete Poisson Equation on Irregular regions", SIAM J. Numer. Anal. 8 pp 722-736.
3. Dendy, J.E. 1982: "Black Box Multigrid", J. Comp. Phys. 48 pp 366-386.
4. Hellerman, S. 1967: "An Updated Estimate of the Wind Stress on the World Ocean", Mon. Wea. Rev., 95 pp 607-626.
5. Hurlburt, H.E. and J. Dana Thompson, 1980: "A Numerical Study of Loop Current Intrusion and Eddy Shedding", J. Phys. Oceanogr. 10 pp 1611-1651.
6. Hurlburt, H.E. and J. Dana Thompson, 1982: "The Dynamics of the Loop Current and Shed Eddies in a Numerical Model of the Gulf of Mexico", in J.C.J. Nihoul (ed), Hydrodynamics of Semi-enclosed Seas, Elsevier Sci. Pub., Amsterdam.
7. Hurlburt, H.E. 1985: "Dynamic Transfer of Simulated Altimeter Data into Subsurface Information by a Numerical Ocean Model", J. Geophys. Res., (in press).
8. Kindle, J.C. 1985: "Sampling Strategy and Model Assimilation of Altimetric Data for Ocean Monitoring and Prediction", J. Geophys. Res., (in press).
9. Leipper, D.F. 1970: "A sequence of current patterns in the Gulf of Mexico", J. Geophys. Res. 75 pp 637-657.
10. Merrell, W.J. and Morrison, J.M. 1981: "On the circulation of the western Gulf of Mexico, with observations from April 1978", J. Geophys. Res. 86 pp 4181-4185.

11. NMC, 1979: "NMC 360/195 Packed Data Fields", Automated Division Staff, National Meteorological Center, Office Note 84,.
12. Rhodes, R.C., J. Dana Thompson and Wallcraft A.J. 1984: "The Navy Corrected Geostrophic Wind data set for the Gulf of Mexico", NORDA tech. rep. (to appear).
13. Rosmond, T.E. 1981: "NOGAPS: Navy Operational Global Atmospheric Prediction System", in Fifth Conference on Numerical Weather Prediction, American Meteorological Society, Boston pp 74-79.
14. Van Wyckhouse, R.J. 1973: "Synthetic Bathymetric Profiling System (SYNBAPS)", Naval Oceanographic Office. Tech. Rep. TR-233.
15. Vukovitch F.M. and Maul G.A. 1984: "Cyclonic eddies in the eastern Gulf of Mexico", J. Phys. Oceanogr. (in press).
16. Wallcraft, A.J. 1985: "Gulf of Mexico Circulation Modeling Study, Annual Progress Report - Year I", prepared for U.S. Dept. of the Interior, Minerals Management Service (contract 14-12-0001-30075).

FIGURE 1: (a) Instantaneous view of the interface deviation in a two layer Gulf of Mexico model driven solely by inflow through the Yucatan Straits. The contour interval is 25 m with solid contours representing downward deviations. (b) Depth of the 22°C isothermal surface, 4-18 August 1966 from Leipper (1970). The contour interval is 25 m.

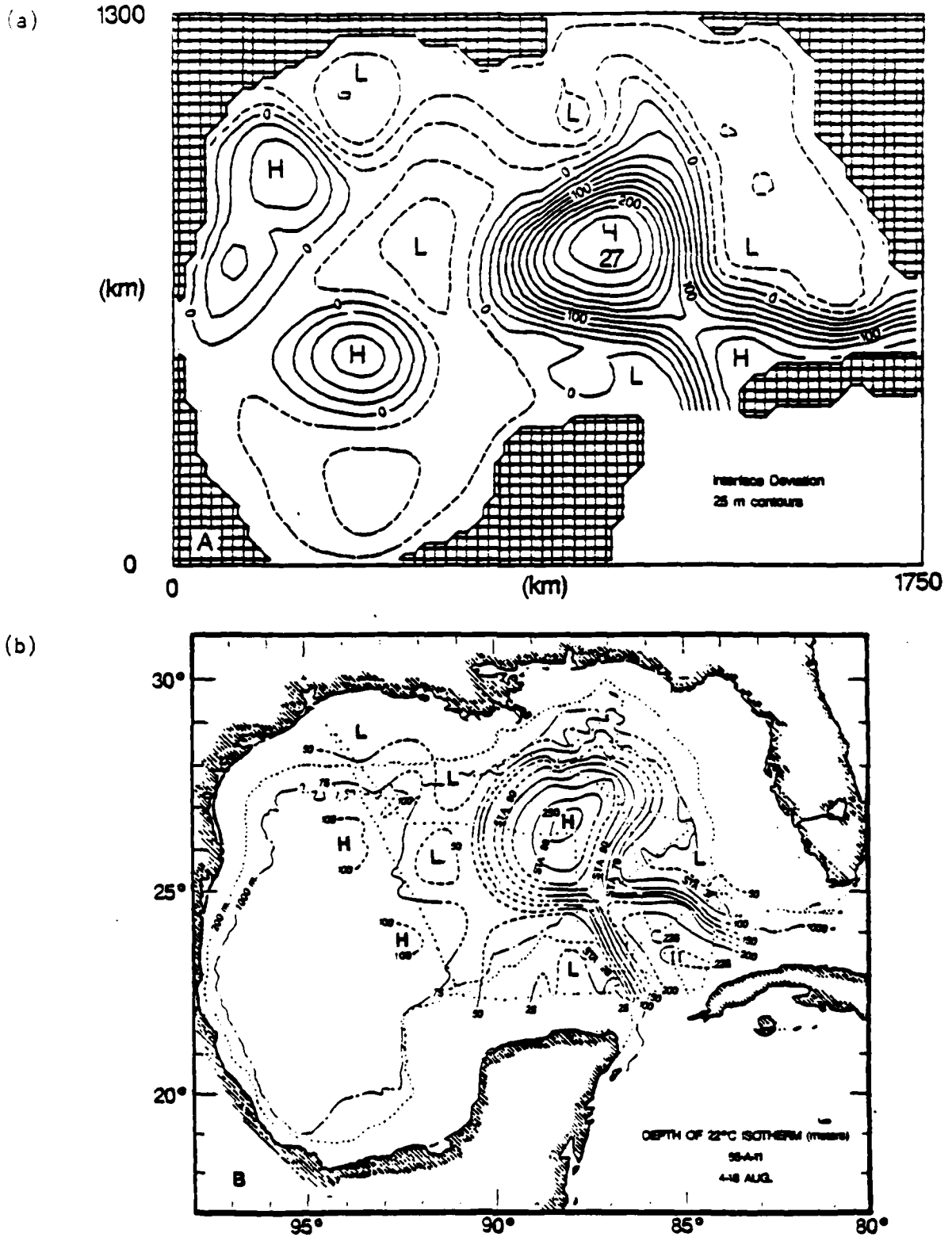
(a)
1300
(km)
0
0
(km)
1750
L
H
27
Interface Deviation
25 m contours
A
(b)
30°
25°
20°
95°
90°
85°
80°
DEPTH OF 22°C ISOTHERM (meters)
4-18 AUG.
B

FIGURE 1

FIGURE 2: (a) Interface deviation from the simulation at day 1970 after an eddy has separated from the model Loop current and propagated westward. (b) Ninety days later the eddy at day 1970 has developed into a counter rotating vortex pair in the western Gulf. The cyclonic vortex is to the north and the anticyclonic to the south. The contour interval is 25 m.

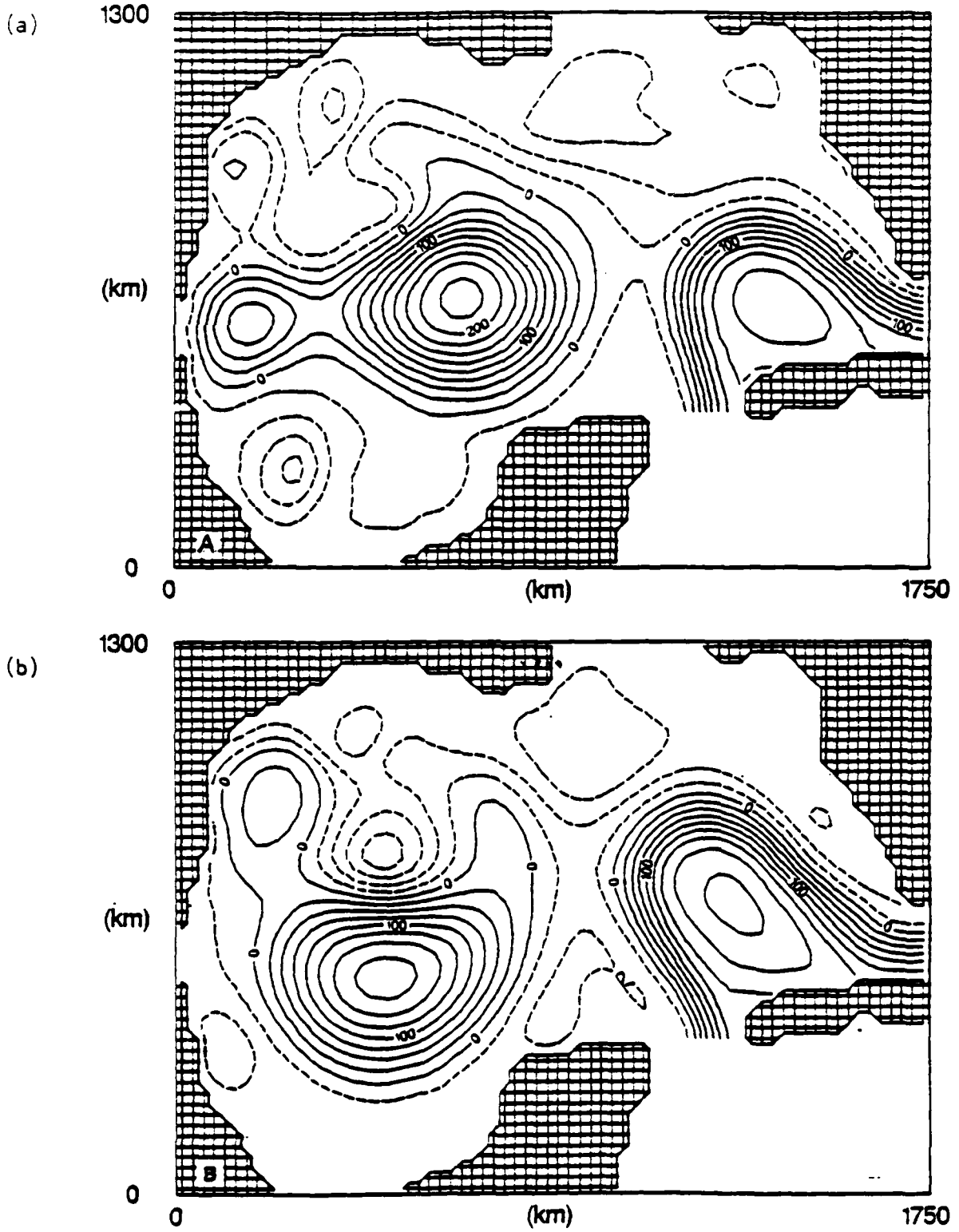

FIGURE 2

FIGURE 3: Counter-rotating vortex pair in the western Gulf of Mexico as shown by the depth of the 15°C isotherm in April 1978. The cyclonic vortex is to the north and the anticyclonic to the south. The contour interval is 25 m, from Merrell and Morrison (1981).

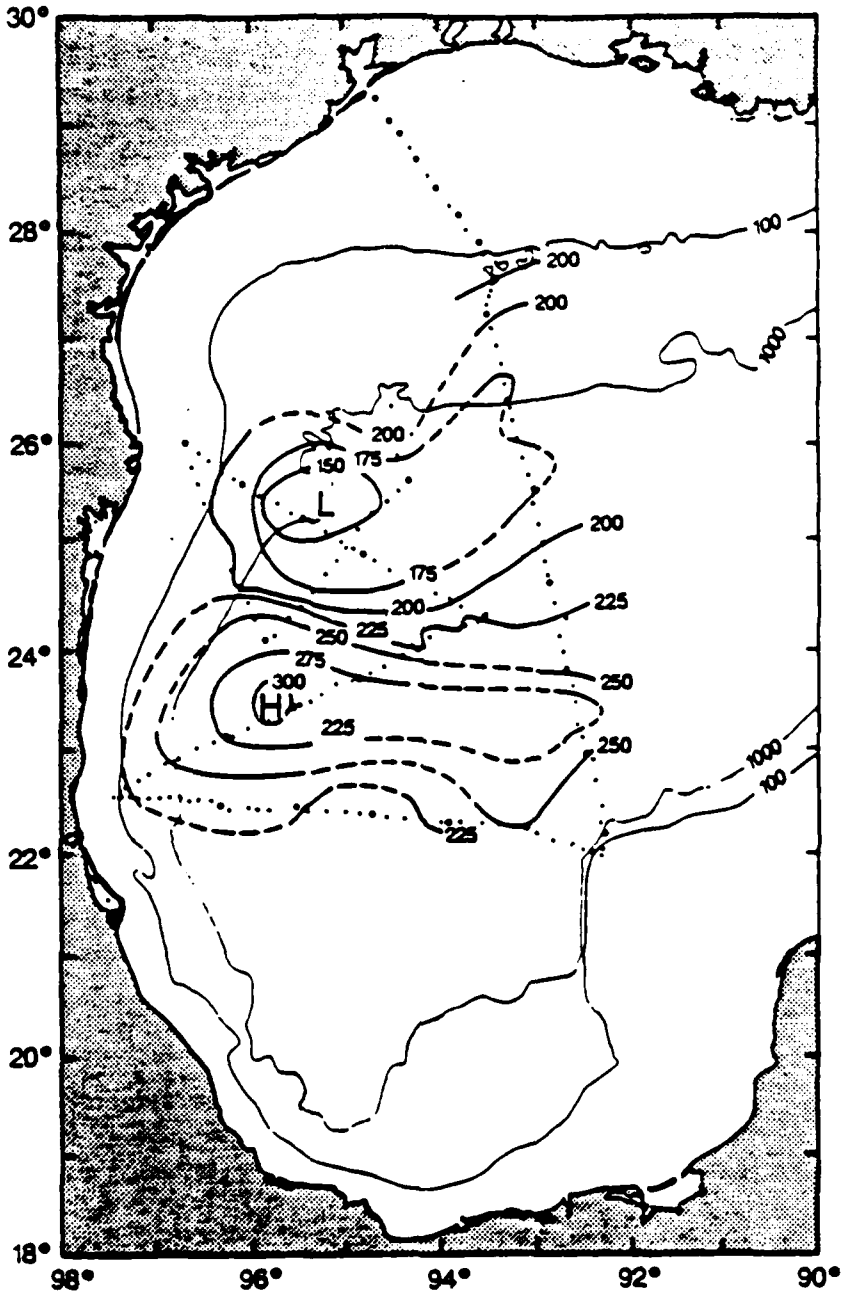
30°
28°
26°
24°
22°
20°
18°
98°
96°
94°
92°
90°
100
200
200
1000
200
150
175
L
175
200
225
200
225
250
275
300
H
225
250
250
1000
100
225

FIGURE 3

FIGURE 4: Winter (a) vector plots of the seasonal climatological wind stresses from ship observations used to drive the model, based on Elliot (1979). Maximum wind stresses shown are about 1.5 dynes in the winter. (b) Corresponding steady state interface deviations from the wind driven model on a 0.2 degree grid. The contour interval is 12.5 m.

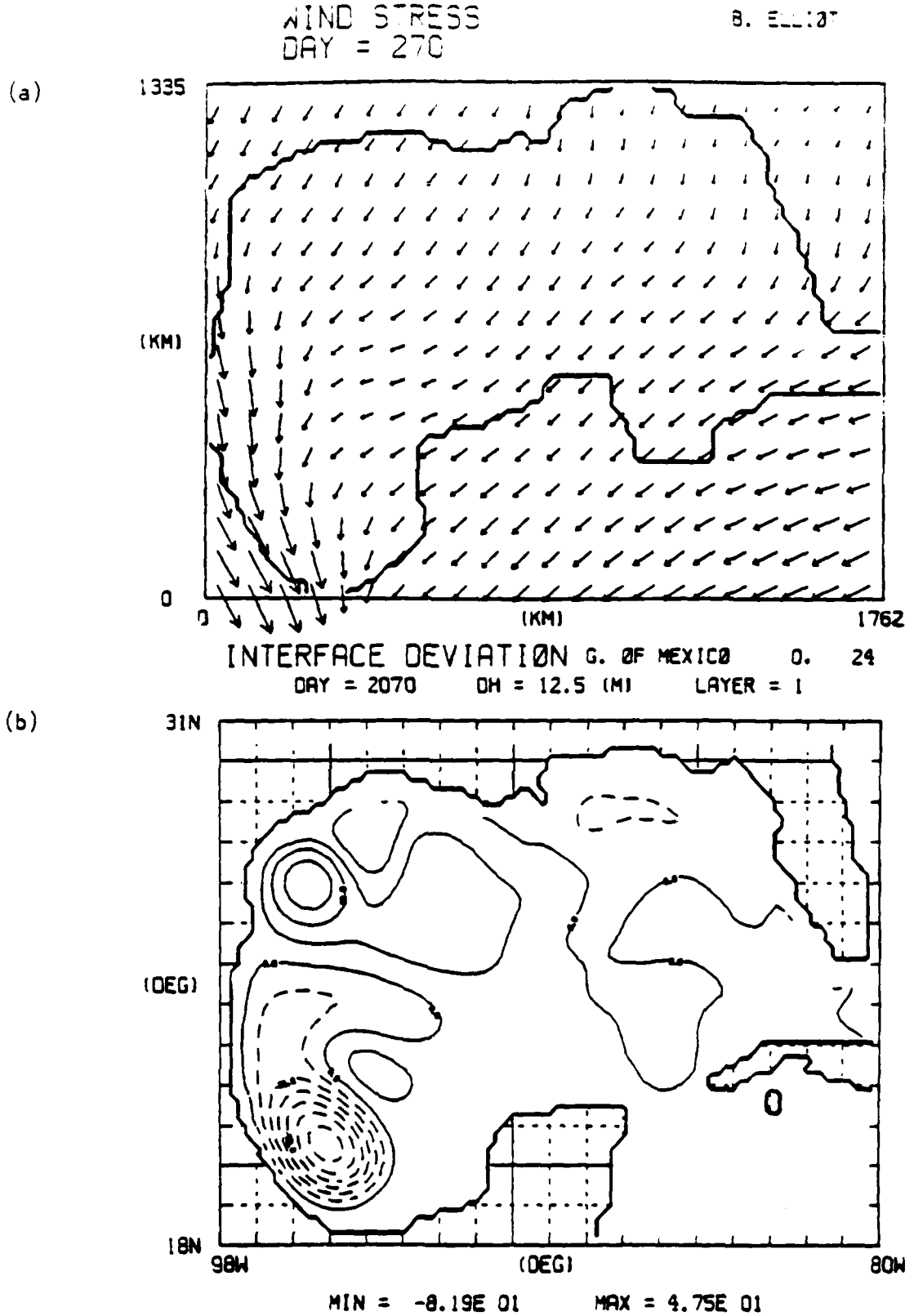
WIND STRESS
DAY = 270
B. ELLIOT
(a)
1335
(KM)
0
0
(KM)
1762
INTERFACE DEVIATION G. OF MEXICO 0. 24
DAY = 2070 DH = 12.5 (M) LAYER = 1
(b)
31N
(DEG)
18N
98W
(DEG)
80W
0
MIN = -8.19E 01 MAX = 4.75E 01

FIGURE 4

FIGURE 5: Spring (a) vector plots of the seasonal climatological wind stresses from ship observations used to drive the model, based on Elliot (1979). Maximum wind stresses shown are about 1.5 dynes in the winter. (b) Corresponding steady state interface deviations from the wind driven model on a 0.2 degree grid. The contour interval is 12.5 m.

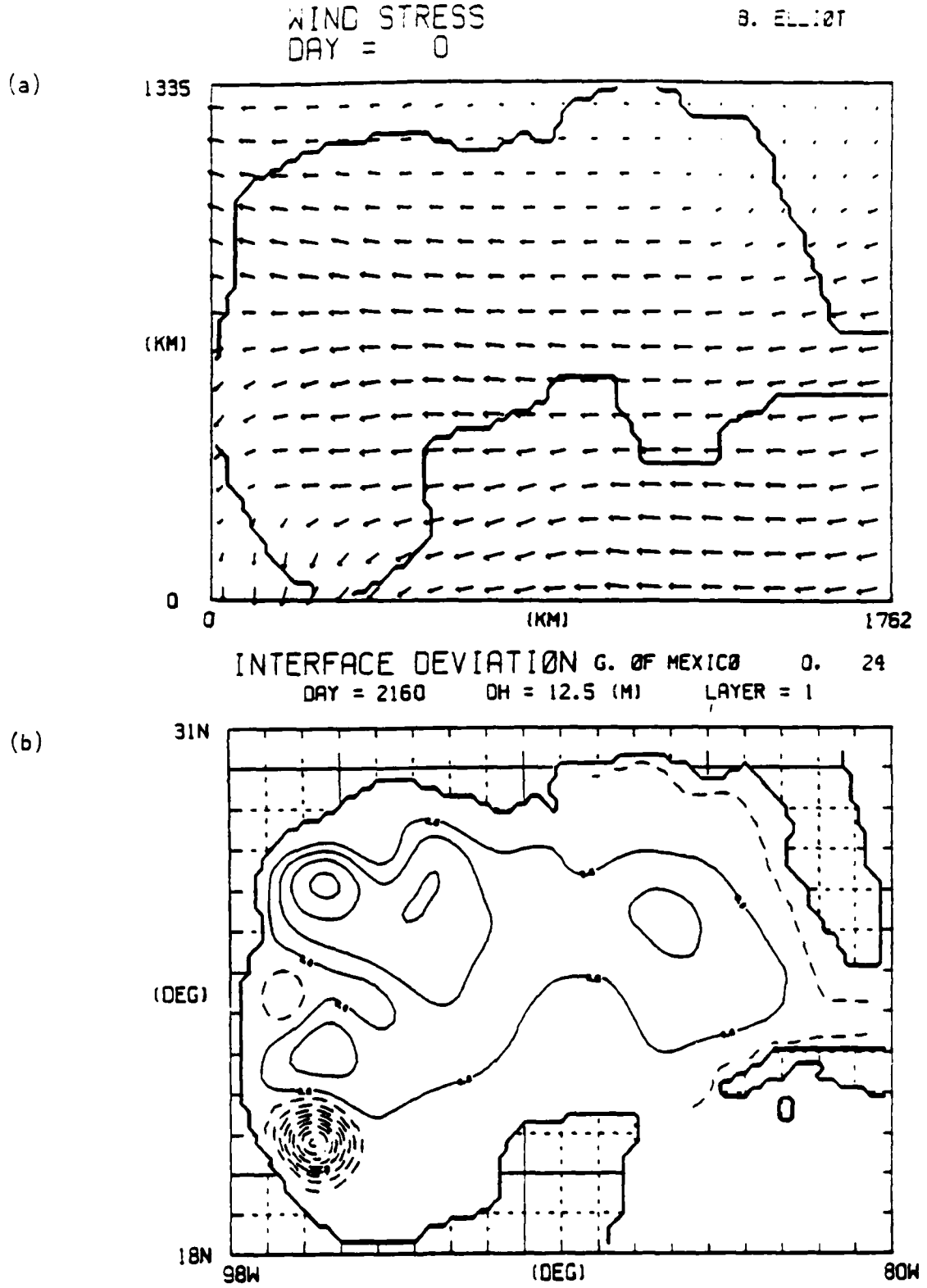
WIND STRESS
DAY = 0
B. ELLIOT
(a)
1335
(KM)
0
0
(KM)
1762
INTERFACE DEVIATIØN G. ØF MEXICØ 0. 24
DAY = 2160 DH = 12.5 (M) LAYER = 1
(b)
31N
(DEG)
18N
98W
(DEG)
80W
0
MIN = -1.15E 02 MAX = 4.10E 01

FIGURE 5

FIGURE 6: Summer (a) vector plots of the seasonal climatological wind stresses from ship observations used to drive the model, based on Elliot (1979). Maximum wind stresses shown are about 1.5 dynes in the winter. (b) Corresponding steady state interface deviations from the wind driven model on a 0.2 degree grid. The contour interval is 12.5 m.

(a)

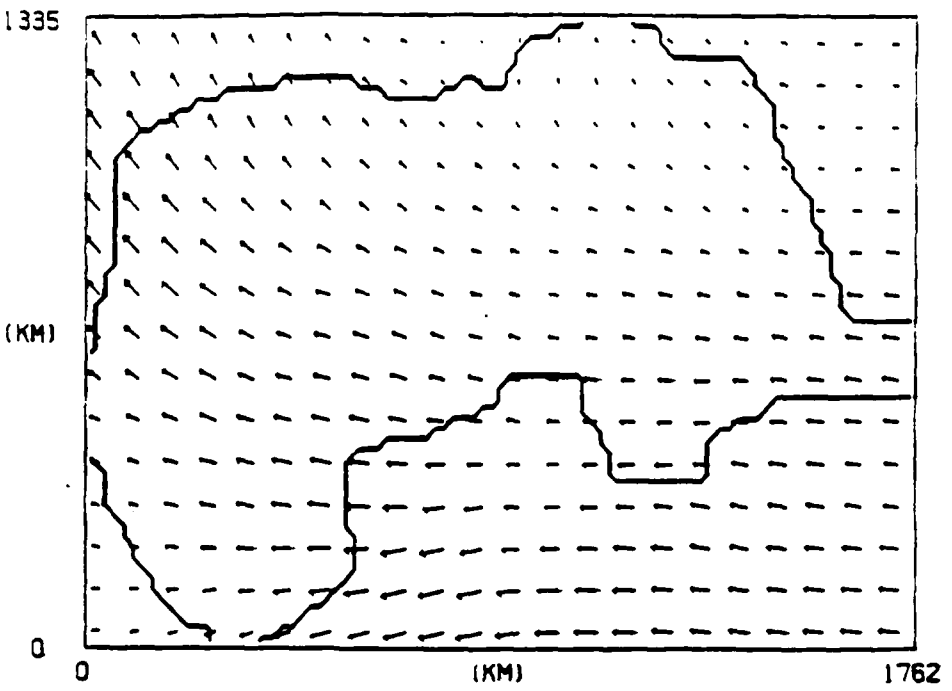
WIND STRESS
DAY = 90
B. ELLIOT
1335
(KM)
0
0
(KM)
1762

(b)

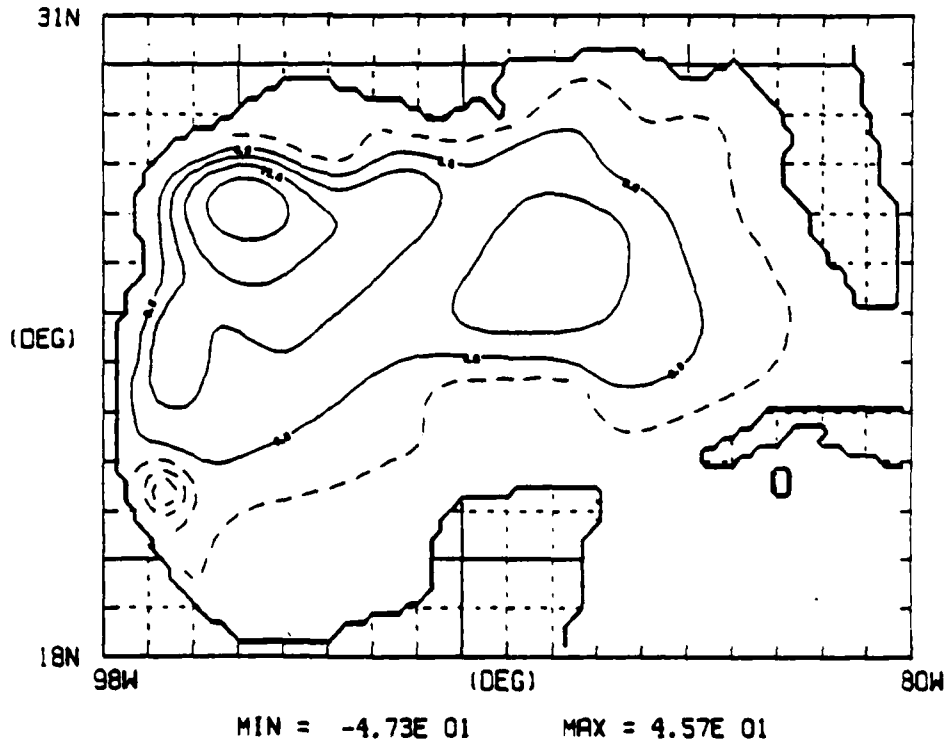
INTERFACE DEVIATION G. OF MEXICO 0. 24
DAY = 1890 DH = 12.5 (M) LAYER = 1
31N
(DEG)
18N
98W
(DEG)
80W
0
MIN = -4.73E 01 MAX = 4.57E 01

FIGURE 6

FIGURE 7: Fall (a) vector plots of the seasonal climatological wind stresses from ship observations used to drive the model, based on Elliot (1979). Maximum wind stresses shown are about 1.5 dynes in the winter. (b) Corresponding steady state interface deviations from the wind driven model on a 0.2 degree grid. The contour interval is 12.5 m.

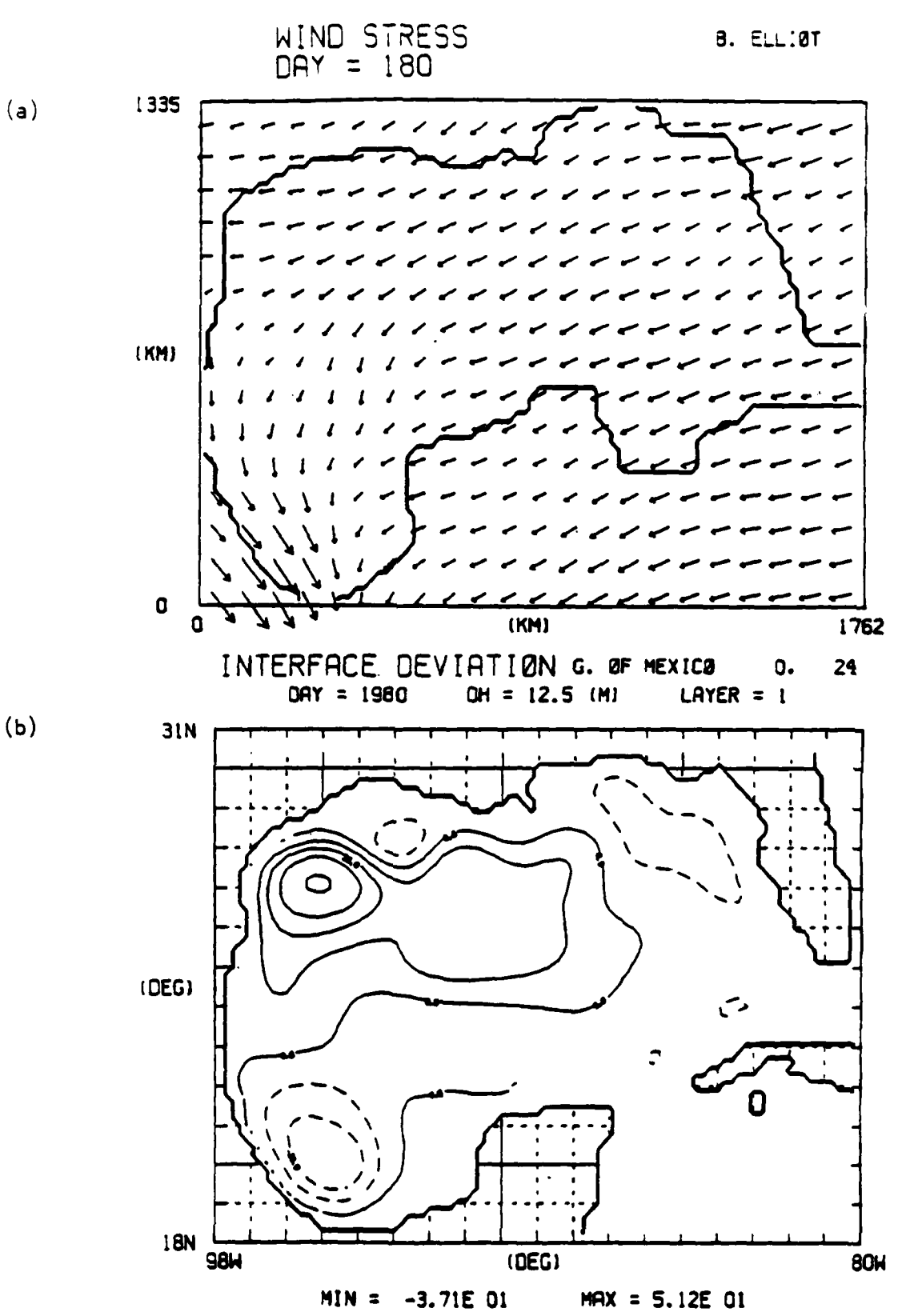
WIND STRESS
DAY = 180
B. ELL:ØT
(a)
1335
(KM)
0
0
(KM)
1762
INTERFACE DEVIATIØN G. ØF MEXICØ 0. 24
DAY = 1980 DH = 12.5 (M) LAYER = 1
(b)
31N
(DEG)
18N
98W
(DEG)
80W
0
MIN = -3.71E 01 MAX = 5.12E 01

FIGURE 7

FIGURE 8: Instantaneous view of the interface deviation every 90 days, from day 90 of model year 9 to day 0 of model year 10, for Experiment 28 (left) and Experiment 34 (right). Experiment 34 is identical to 28 except for the addition of wind forcing. The contour interval is 25 m.

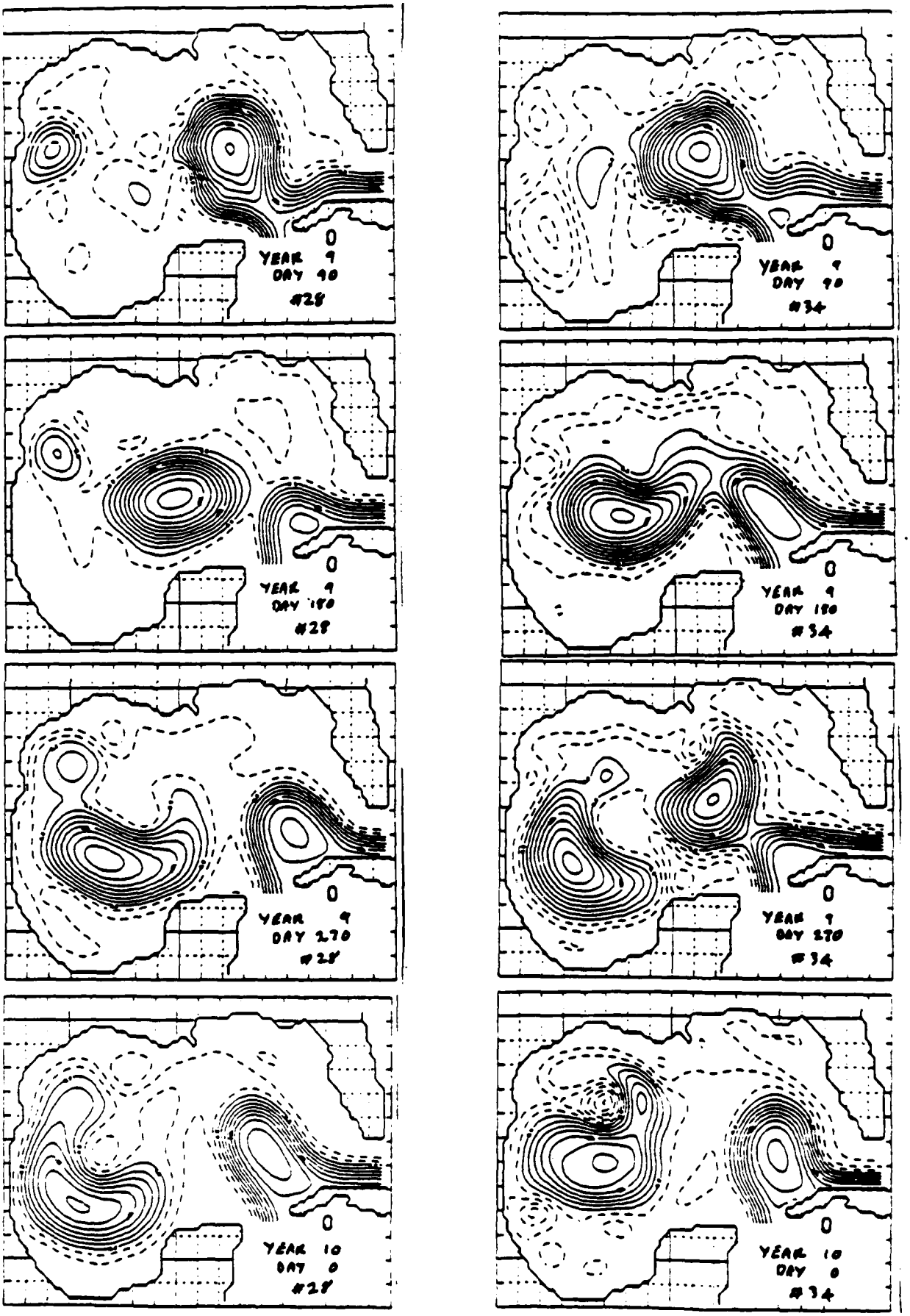
0
YEAR 9
DAY 90
#28
0
YEAR 9
DAY 90
#34
0
YEAR 9
DAY 180
#28
0
YEAR 9
DAY 180
#34
0
YEAR 9
DAY 270
#28
0
YEAR 9
DAY 270
#34
0
YEAR 10
DAY 0
#28
0
YEAR 10
DAY 0
#34

FIGURE 8

FIGURE 9: Instantaneous view of the interface deviation every 20 days, from day 260 of model year 9 to day 0 of model year 10, for Experiment 34.

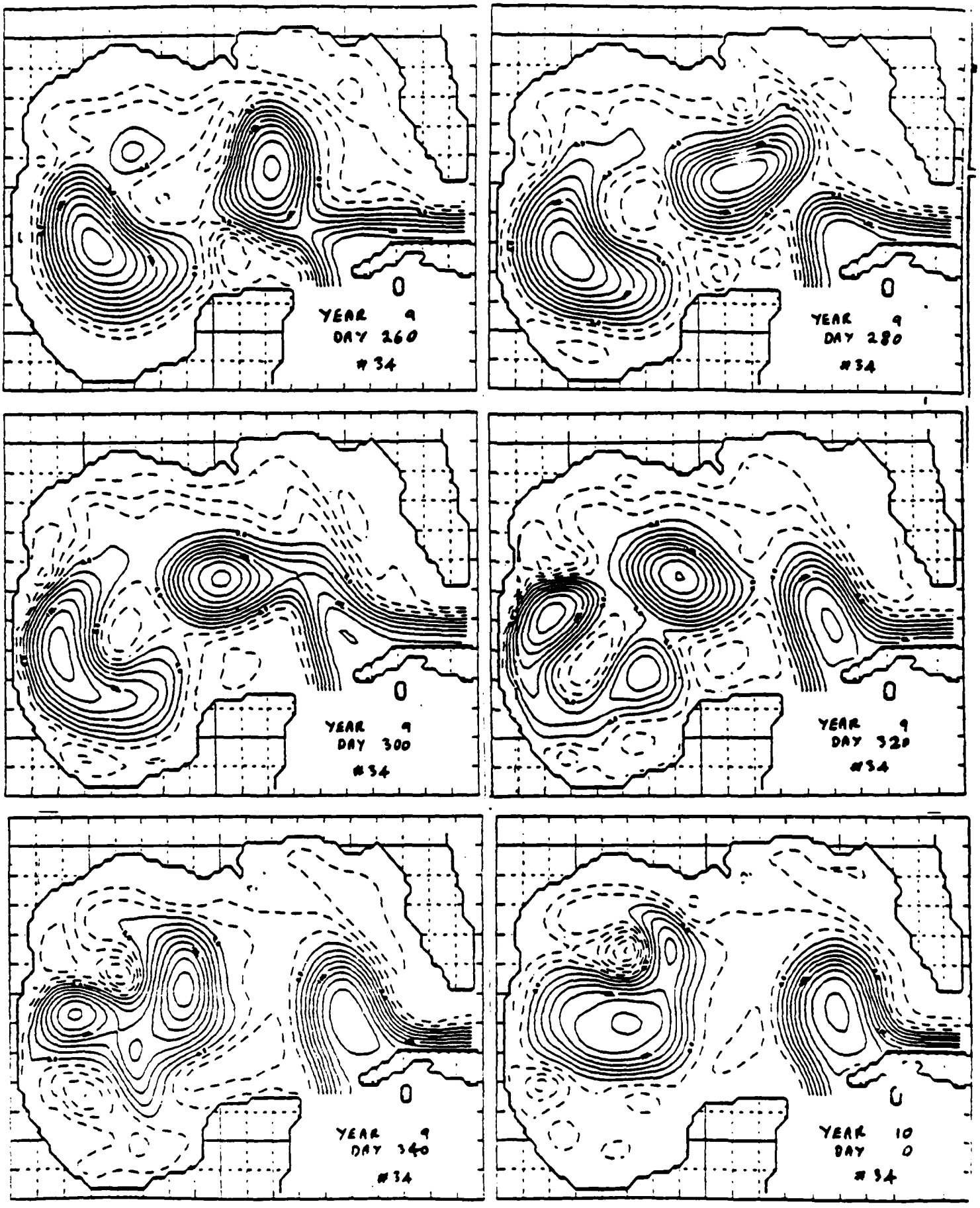
0
YEAR 9
DAY 260
#34
0
YEAR 9
DAY 280
#34
0
YEAR 9
DAY 300
#34
0
YEAR 9
DAY 320
#34
0
YEAR 9
DAY 340
#34
0
YEAR 10
DAY 0
#34

FIGURE 9

FIGURE 10: Interface deviation mean and variability, for the Gulf of Mexico from ocean model. (a) Experiment 31, wind forcing only; (b) Experiment 28, port forcing only; (c) Experiment 34 wind plus port forcing. The contour interval is 12.5 m.

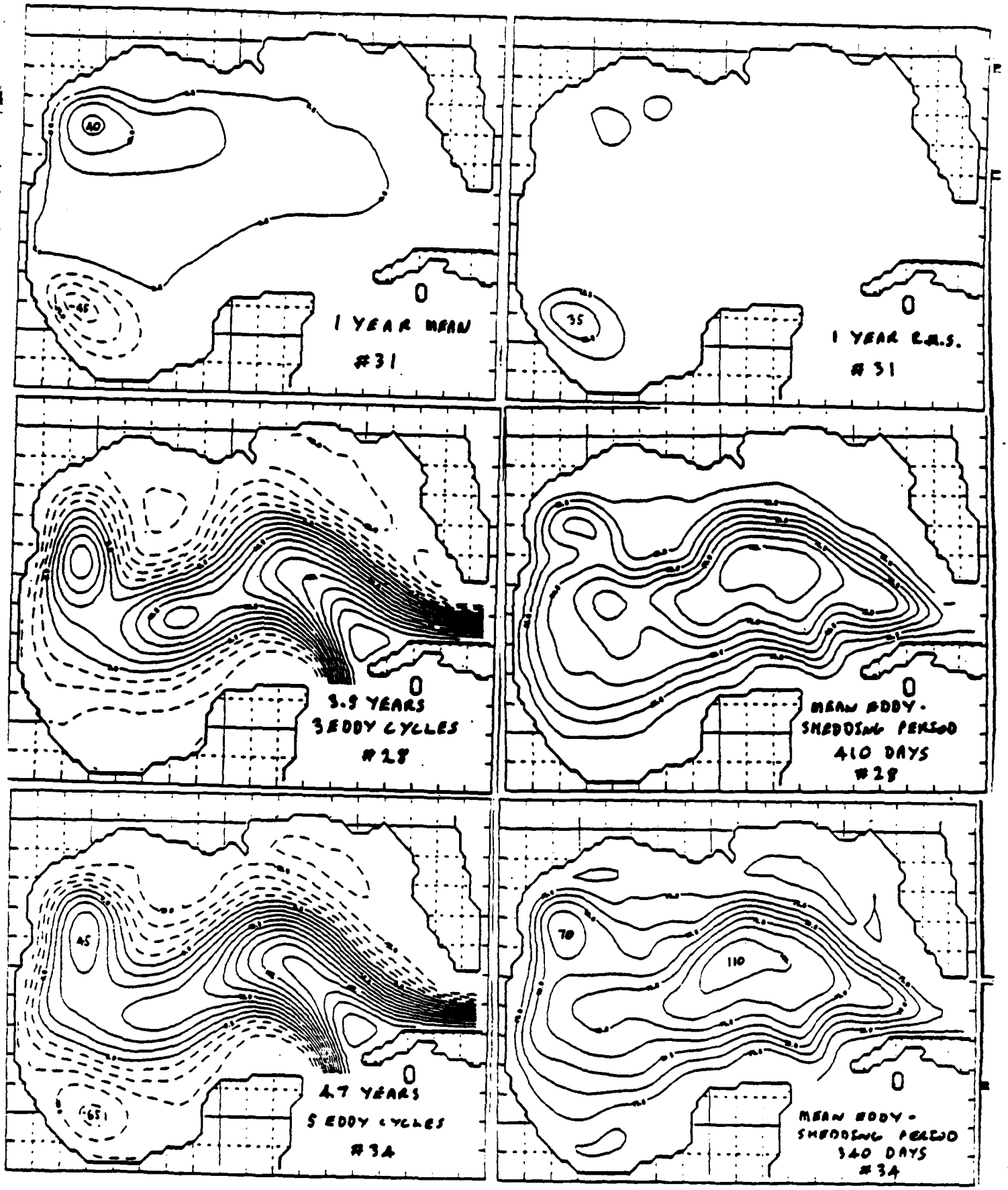
40
-45
0
1 YEAR MEAN
#31
35
0
1 YEAR R.M.S.
#31
0
3.9 YEARS
3 EDDY CYCLES
#28
0
MEAN EDDY-
SHEDDING PERIOD
410 DAYS
#28
45
(65)
0
4.7 YEARS
5 EDDY CYCLES
#34
70
110
0
MEAN EDDY-
SHEDDING PERIOD
340 DAYS
#34

FIGURE 10

FIGURE 11: Bottom topography and coastline geometry for North Atlantic model on 0.25 by 0.2 degree grid. The contour interval is 500 m and the shallowest depth is 1000 m. The topography is from SYNBAPS, but has been smoothed twice to remove small scale noise.

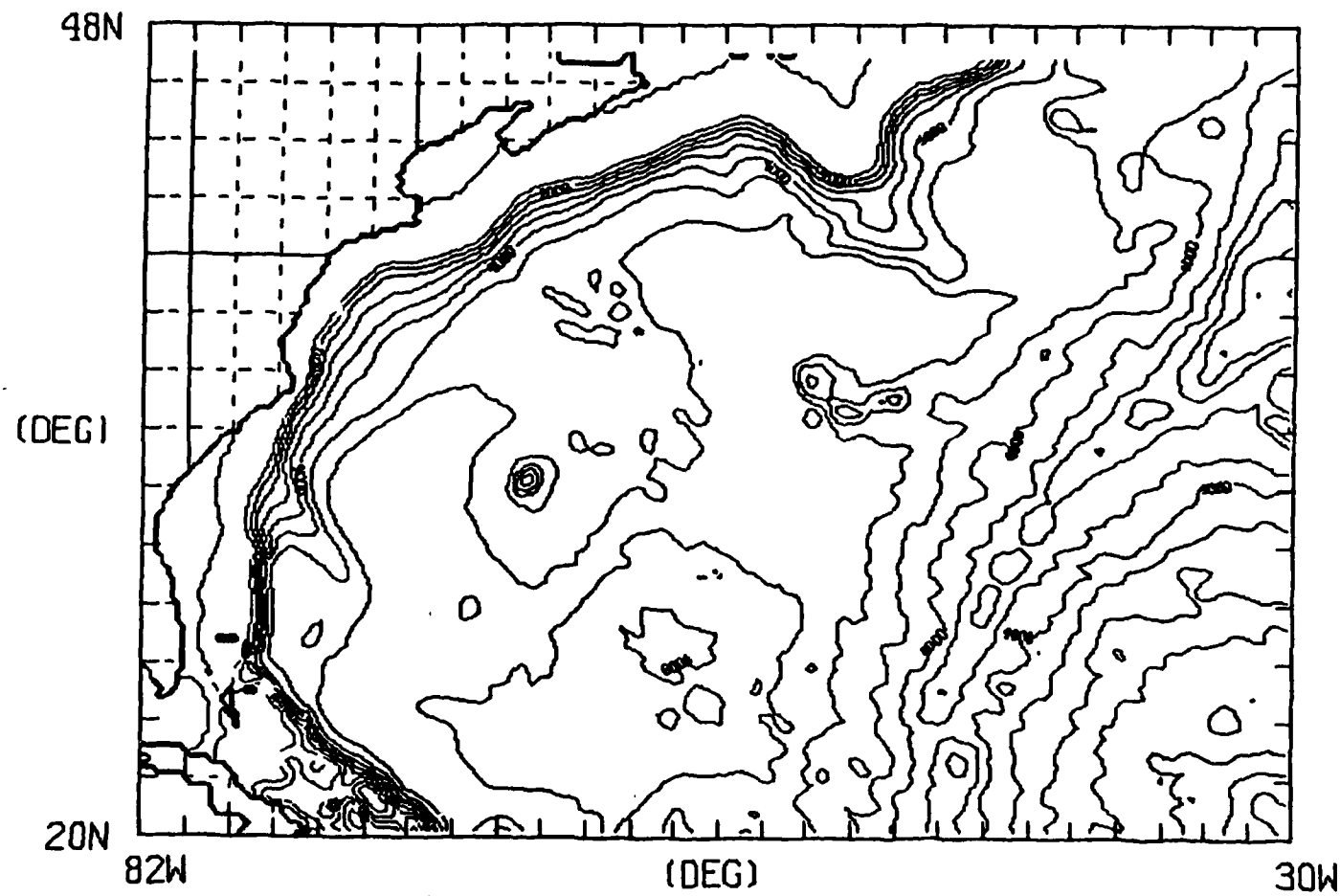
MØDEL LABEL = 511
V. S. NØRTH ATLANTIC (SMØØTH=2).
DX,DY = 0.250,0.200 (DEG) DBT = 500.0 (M)
48N
(DEG)
20N
82W
(DEG)
30W

FIGURE 11

FIGURE 12: (a) Instantaneous view of the interface deviation in a two-layer simulation of the North Atlantic driven from rest to statistical equilibrium solely by monthly climatological winds. The contour interval is 25 m, with solid contours representing downward deviations.

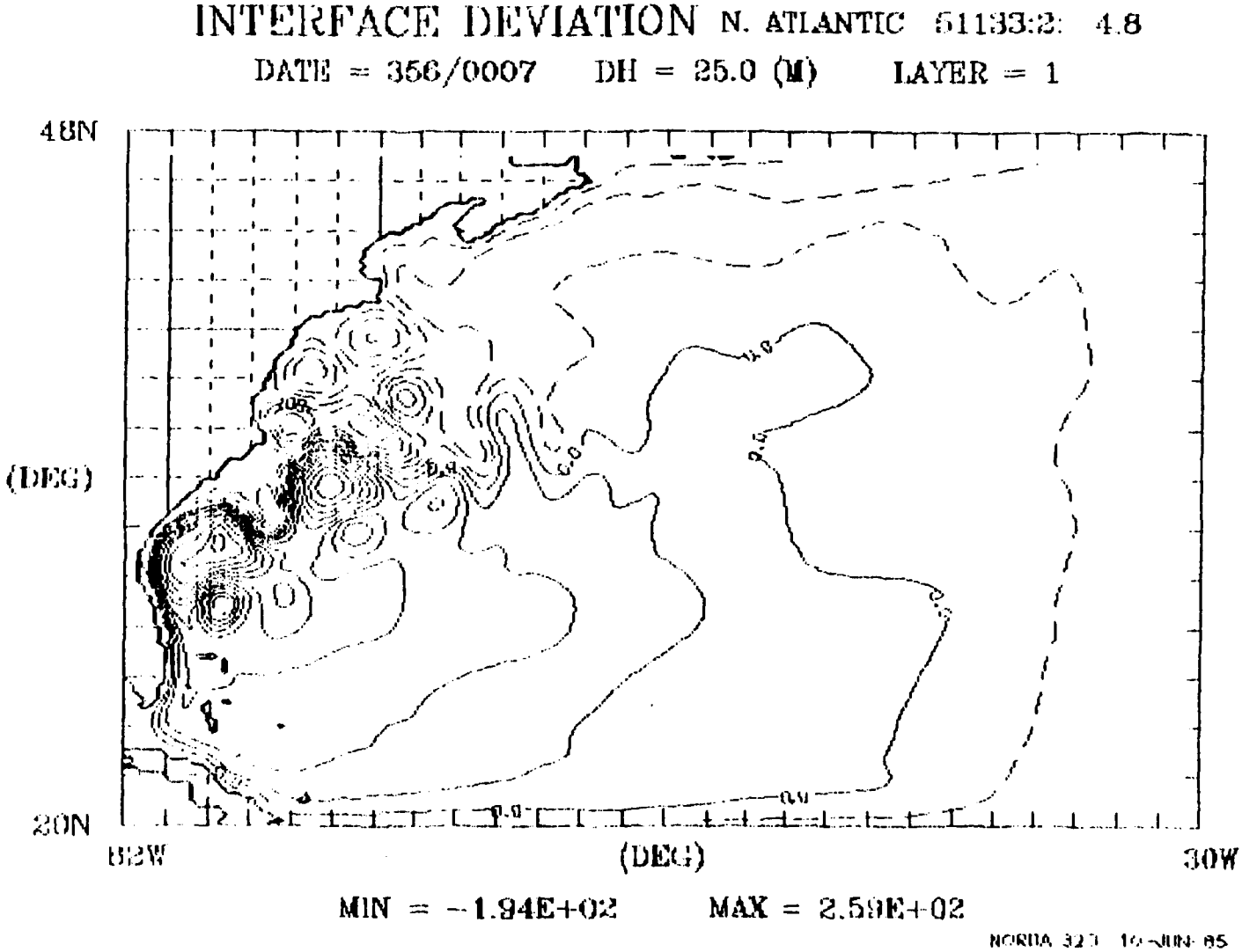
INTERFACE DEVIATION N. ATLANTIC 51133:2: 4.8
DATE = 356/0007 DH = 25.0 (M) LAYER = 1
48N
(DEG)
20N
82W
(DEG)
30W
MIN = -1.94E+02 MAX = 2.59E+02
NORDA 323 10-JUN-85

FIGURE 12

FIGURE 13: Bottom topography and coastline geometry for Gulf of Mexico model on 0.1 degree grid. The contour interval is 500 m and the shallowest depth is 500 m. This is the raw topography field from SYNBAPS, it is not suitable for direct use in an ocean model.

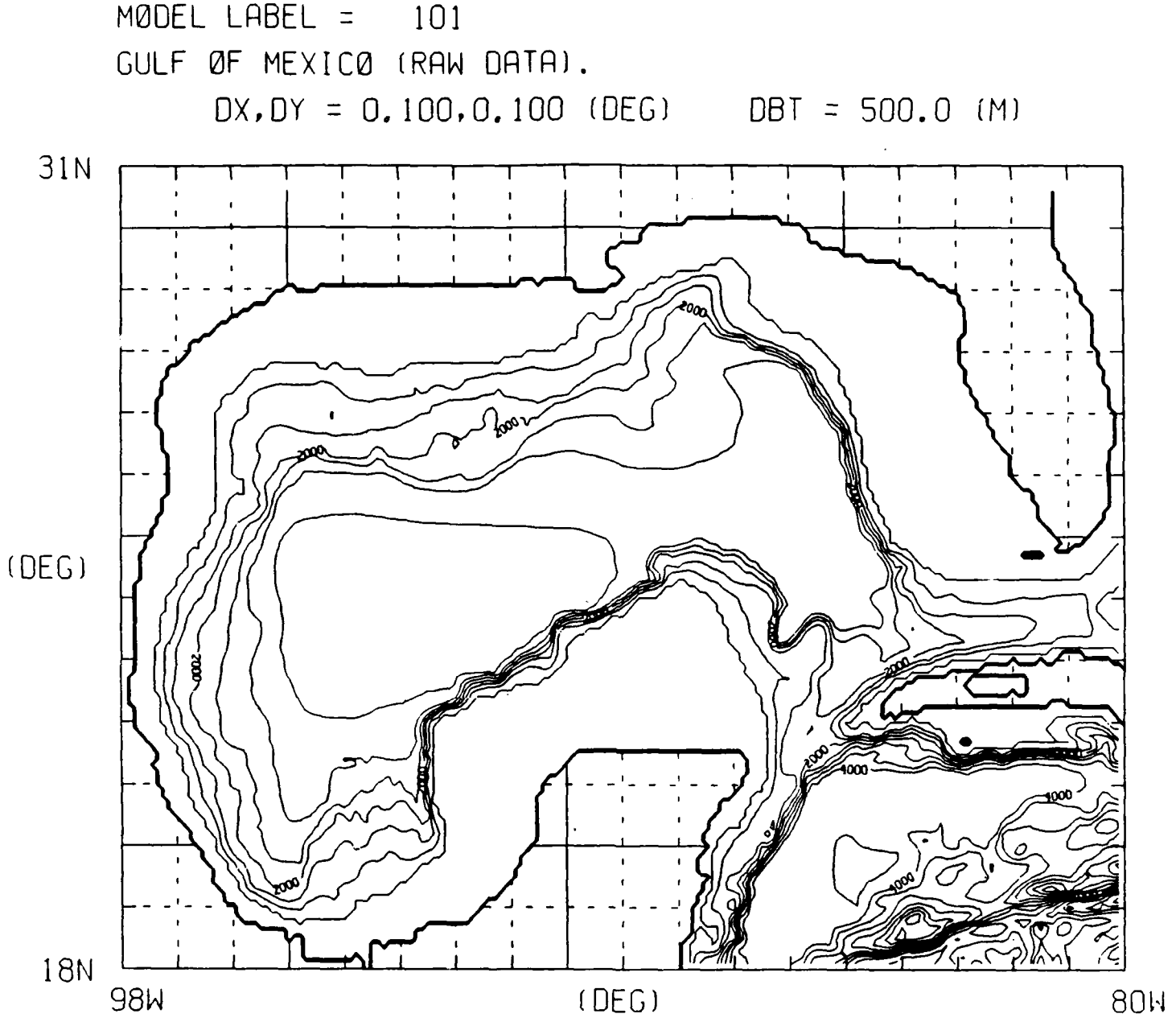
MØDEL LABEL = 101
GULF ØF MEXICØ (RAW DATA).
DX,DY = 0.100,0.100 (DEG) DBT = 500.0 (M)
31N
(DEG)
18N
98W
(DEG)
80W
2000
2000
2000
2000
2000
2000
1000
1000
1000

FIGURE 13

FIGURE 14: Bottom topography and coastline geometry for Gulf of Mexico model on 0.1 degree grid. The contour interval is 500 m and the shallowest depth is 500 m. The topography is based on that in Figure 13, but is now in a form suitable for use in the ocean model.

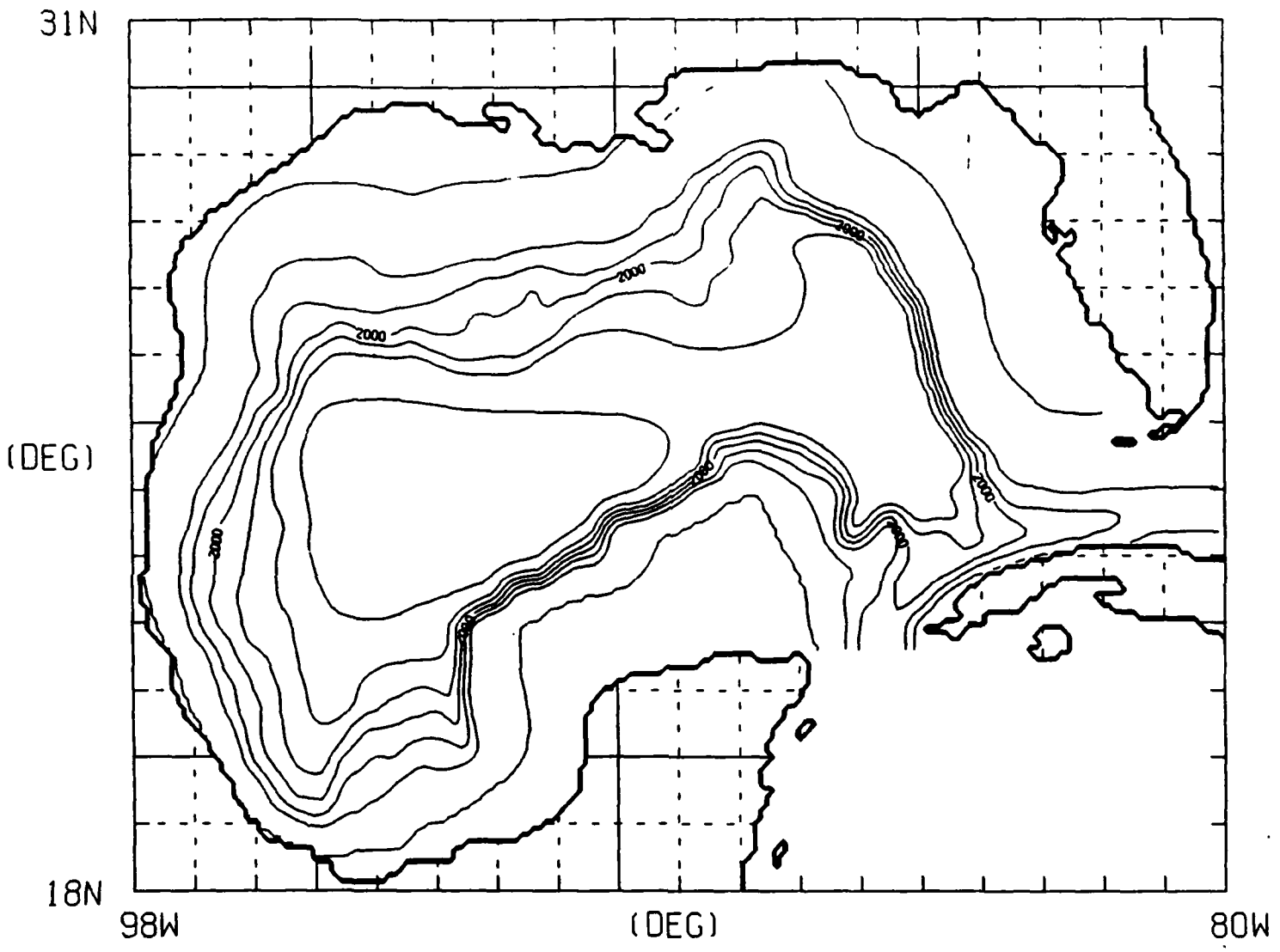
MØDEL LABEL = 101
GULF ØF MEXICØ (SMØØTH=2).
DX,DY = 0.100,0.100 (DEG) DBT = 500.0 (M)
31N
(DEG)
18N
98W
(DEG)
80W
2000
2000
2000
2000
2000
2000

FIGURE 14

FIGURE 15: (a)NOGAPS mean wind stress curl for January 1983.
(b)NOGAPS mean wind stress curl for April 1983.
(c)NOGAPS mean wind stress curl for July 1983.
(d)NOGAPS mean wind stress curl for October 1983.

WIND STRESS CLIMATOGRAPHY (1983)

CURL

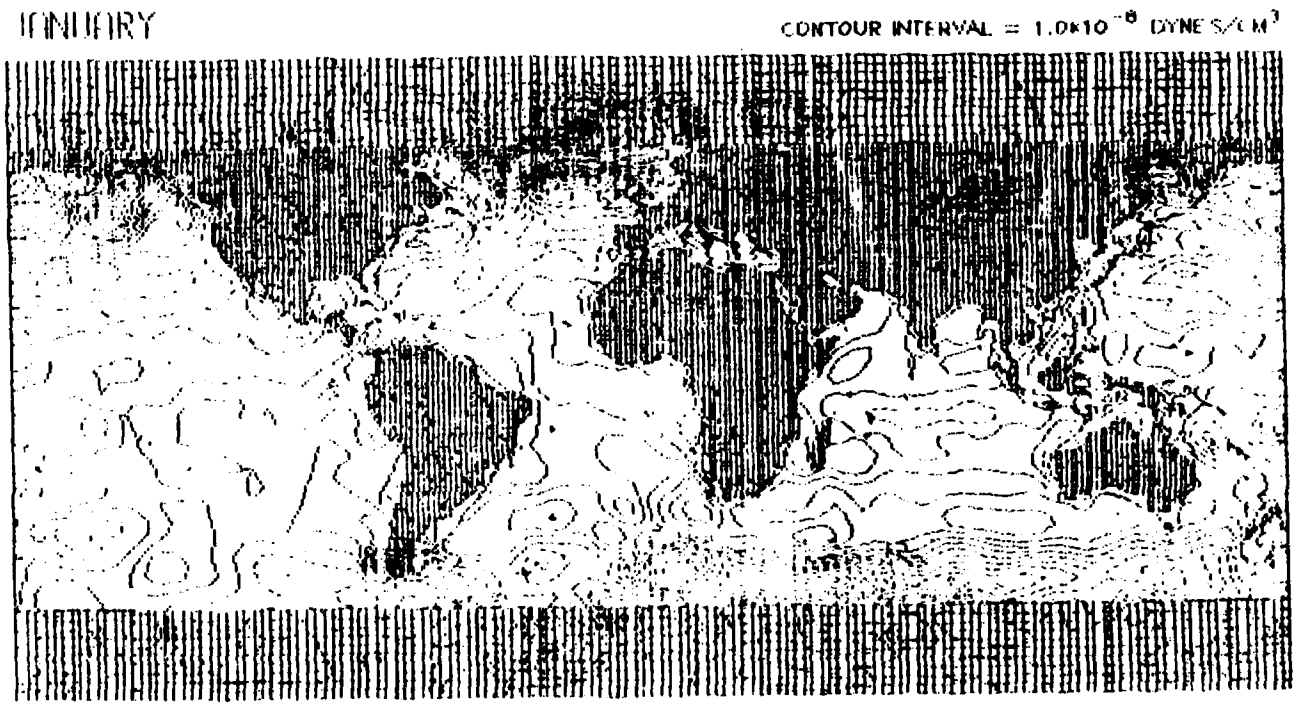

FIGURE 15(a)

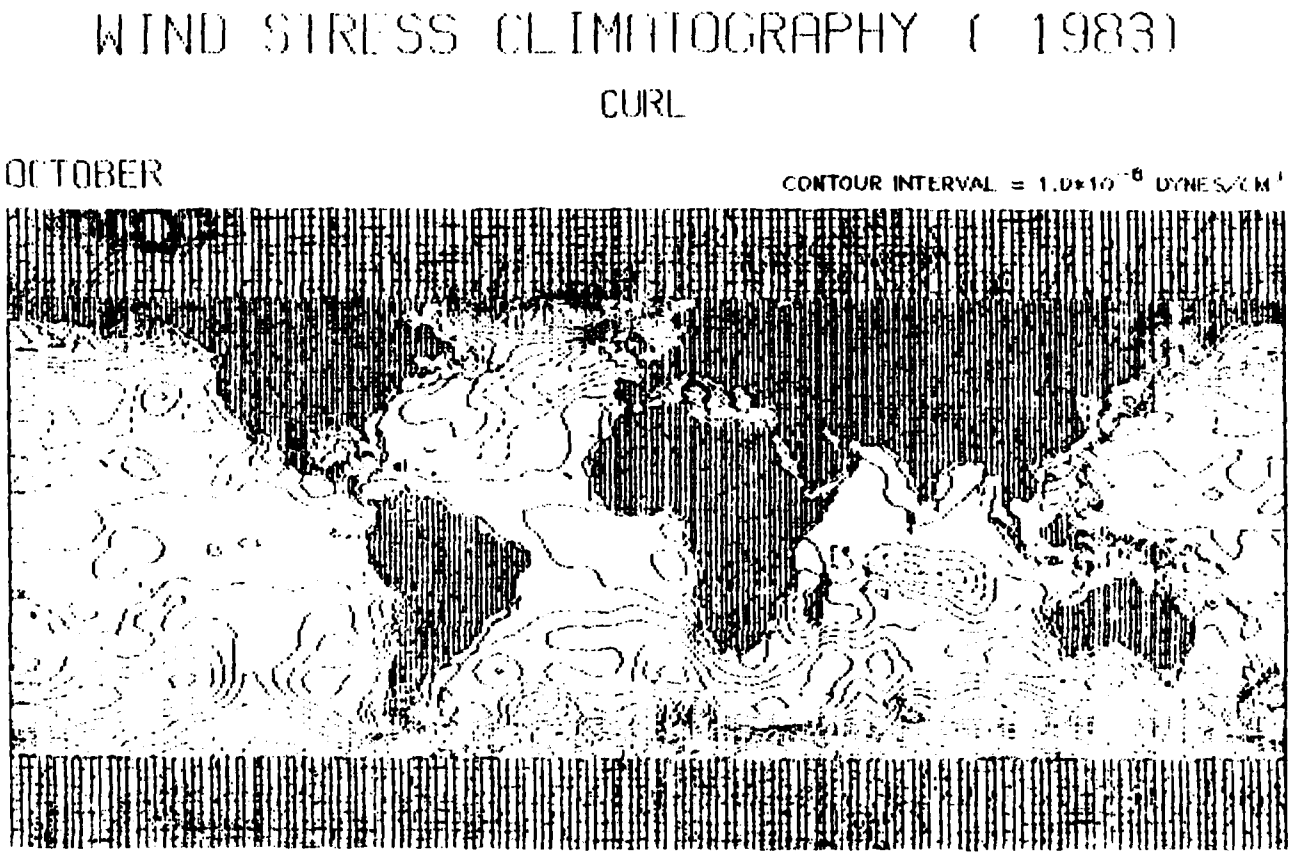
WIND STRESS CLIMATOGRAPHY (1983)
CURL
OCTOBER
CONTOUR INTERVAL = 1.0*10 -6 DYNES/CM 3

FIGURE 15(d)

WIND STRESS CLIMATOGRAPHY (1983)

CURL

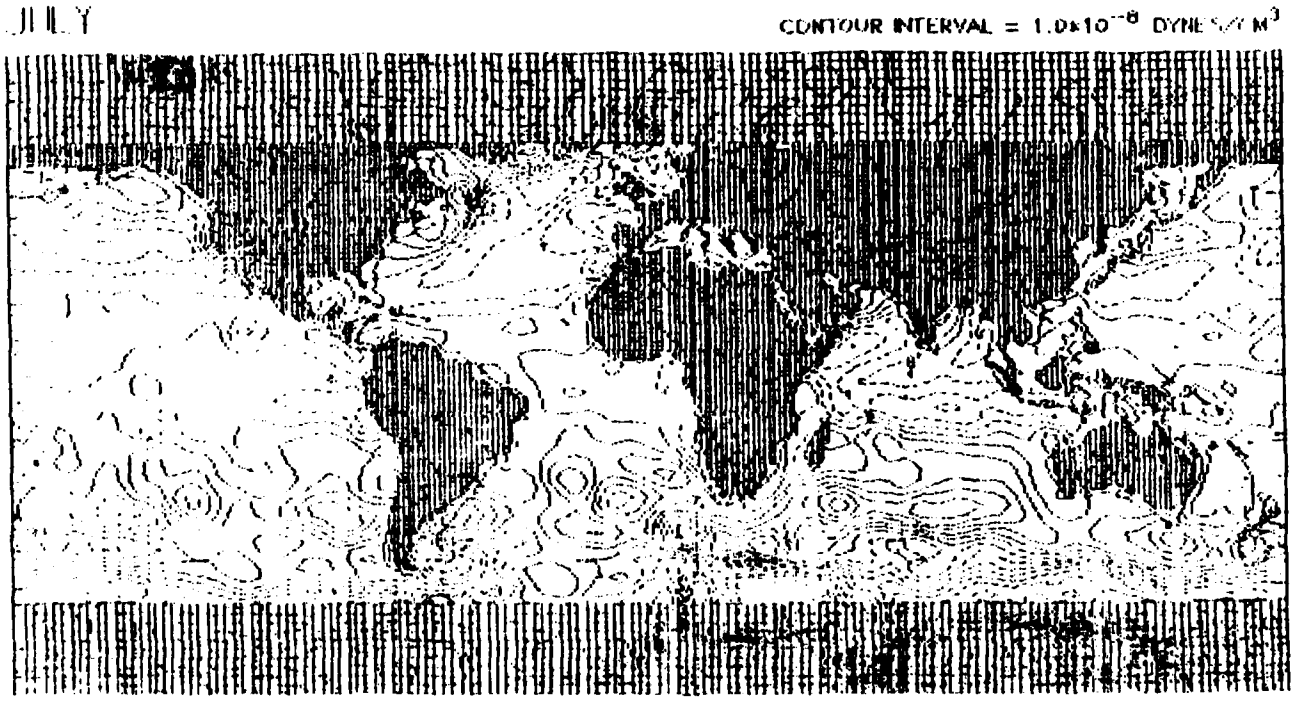

FIGURE 15(c)

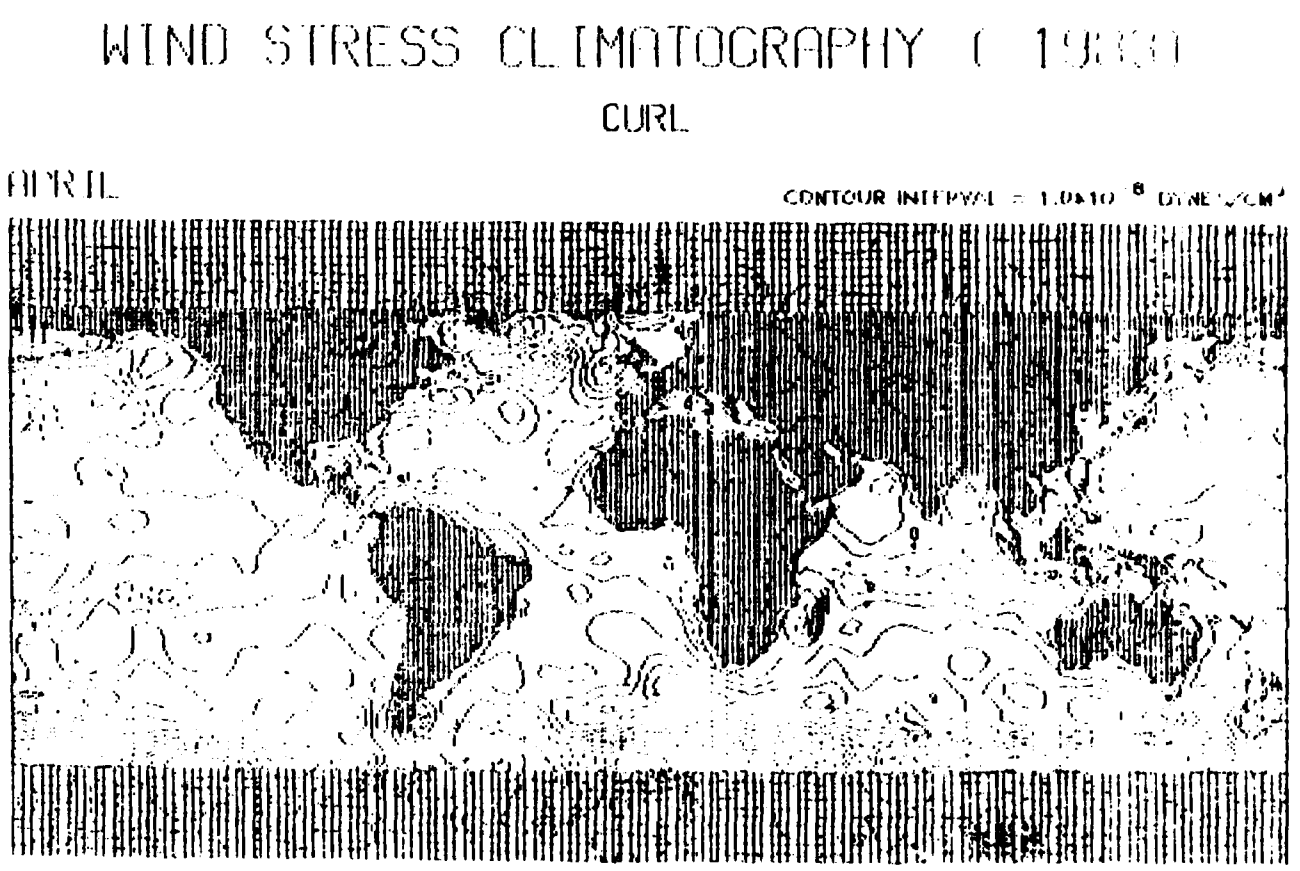
WIND STRESS CLIMATOGRAPHY (19
CURL
APRIL
CONTOUR INTERVAL = 1.0X10 -8 DYNE/CM3

FIGURE 15(b)

FIGURE 16: (a)Hellerman climatological wind stress curl for January.
(b)Hellerman climatological wind stress curl for April.
(c)Hellerman climatological wind stress curl for July.
(d)Hellerman climatological wind stress curl for October.

WIND STRESS CLIMATOGRAPHY

CURL

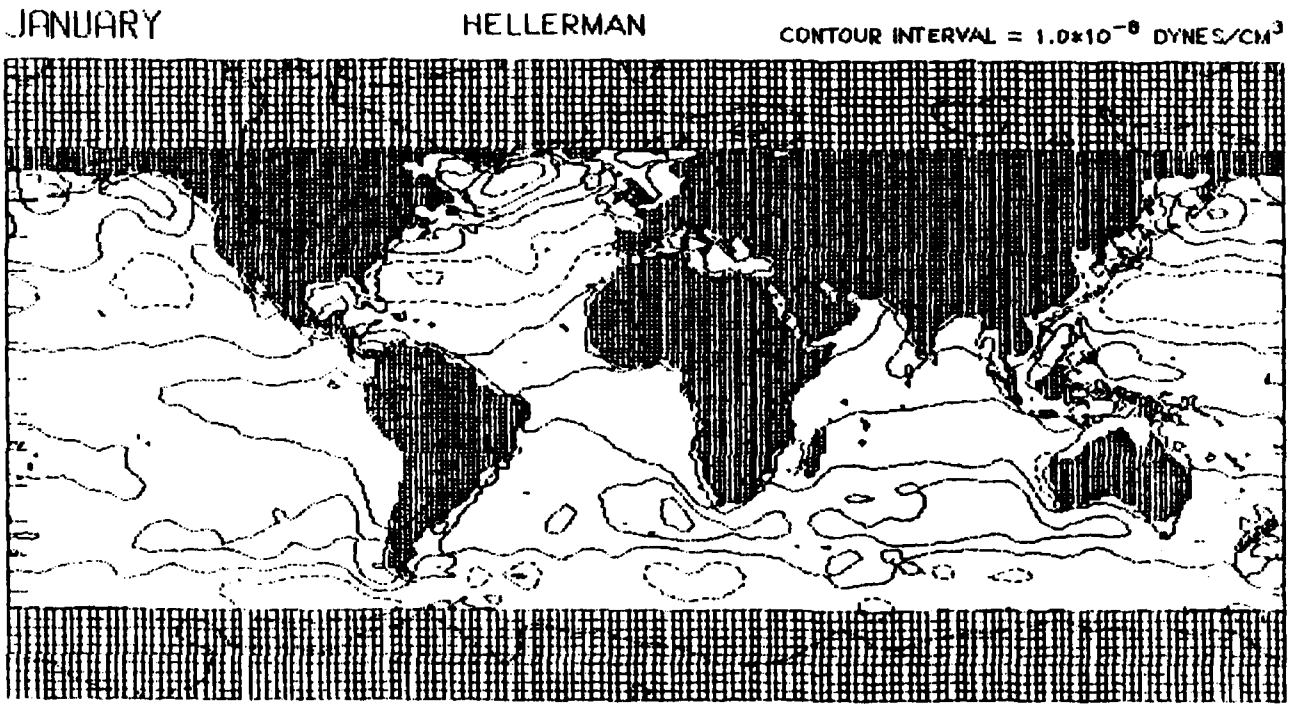

FIGURE 16(a)

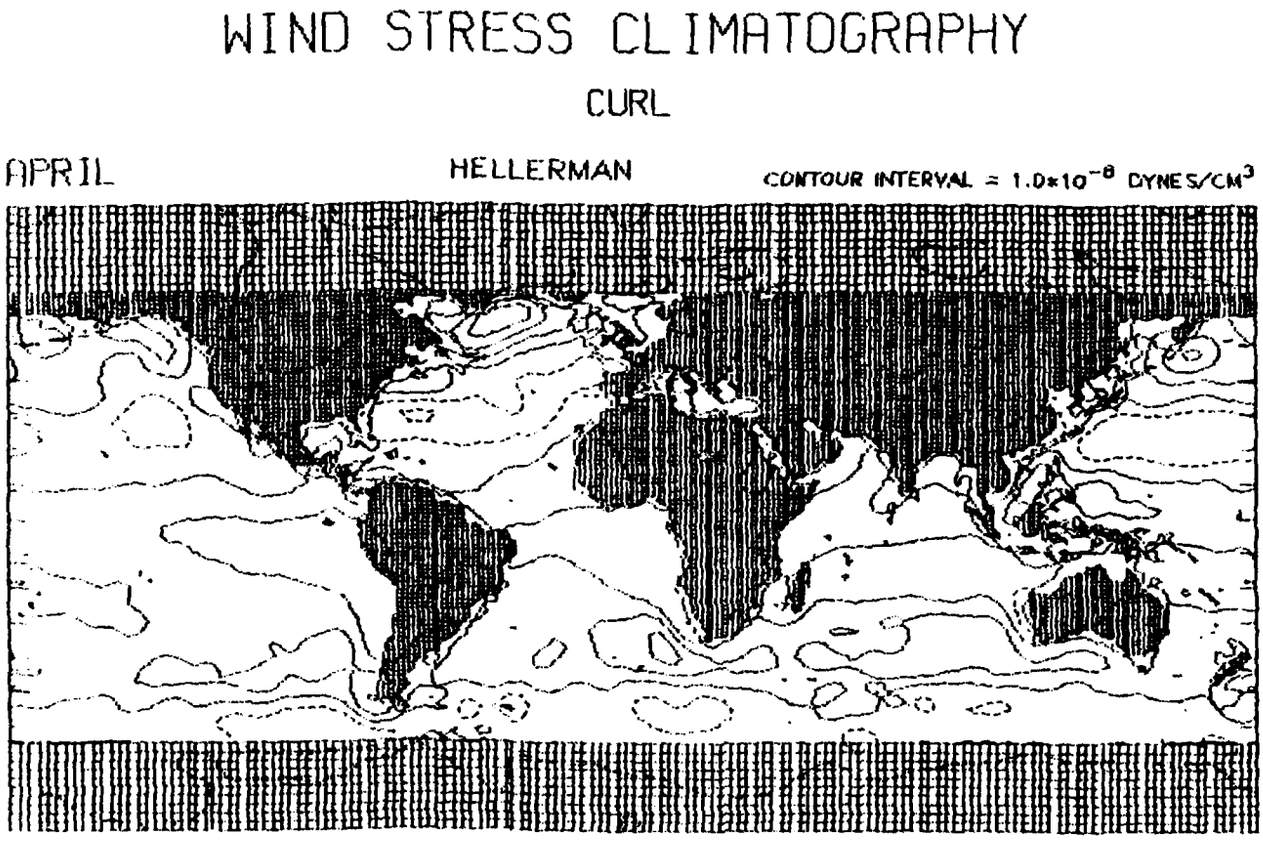
WIND STRESS CLIMATOGRAPHY
CURL
APRIL
HELLERMAN
CONTOUR INTERVAL = 1.0×10⁻⁸ DYNES/CM³

FIGURE 16(b)

WIND STRESS CLIMATOGRAPHY

CURL

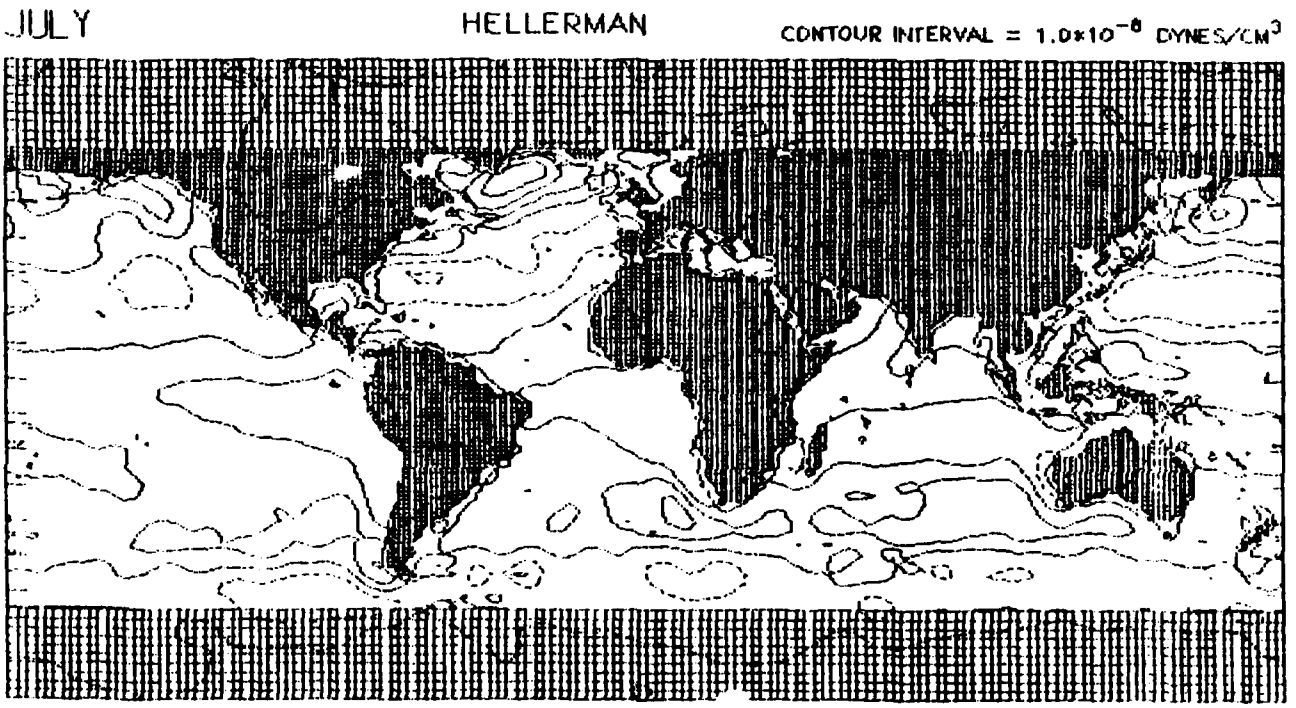

FIGURE 16(c)

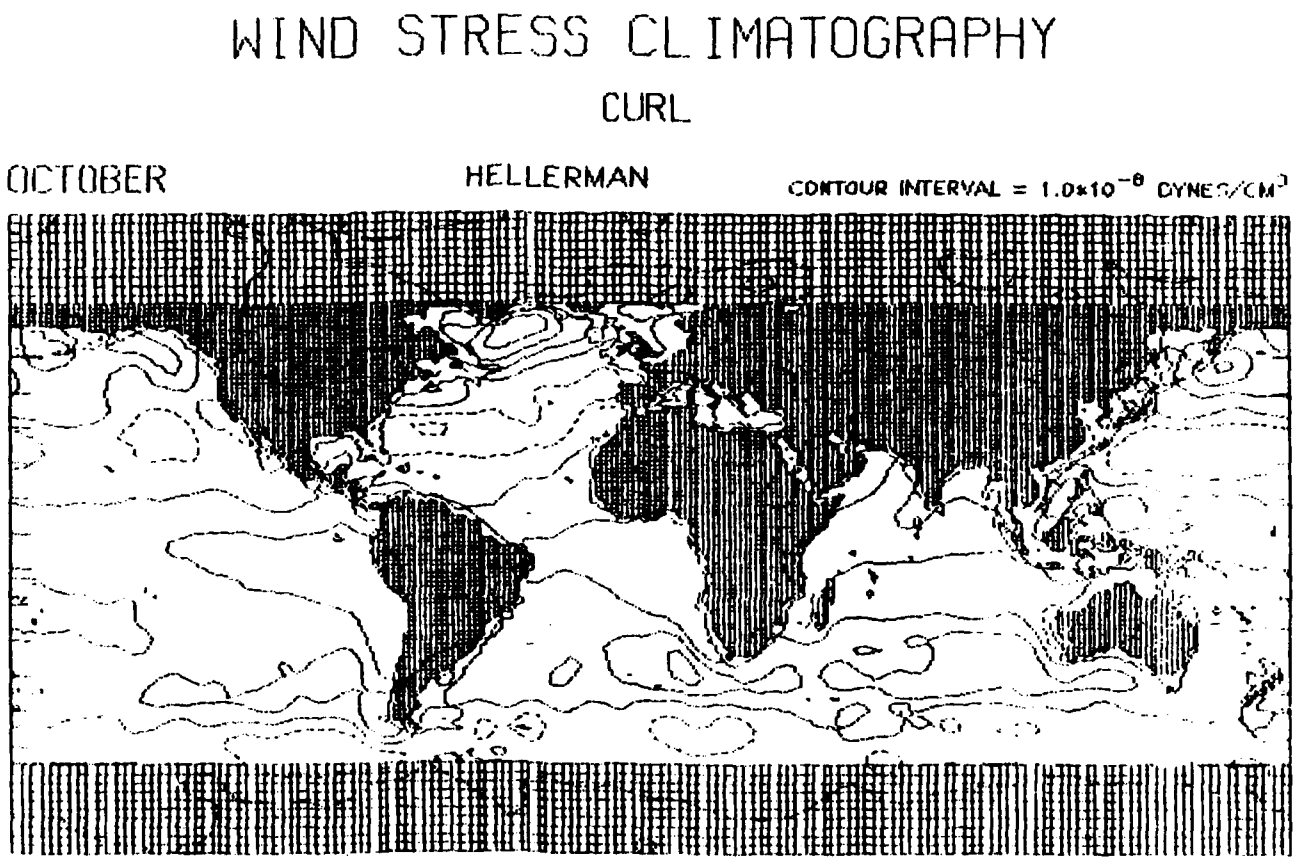
WIND STRESS CLIMATOGRAPHY
CURL
OCTOBER
HELLERMAN
CONTOUR INTERVAL = 1.0*10^-8 DYNES/CM^3

FIGURE 16(d)

FIGURE 17: (a)NORAPS mean wind stress for October 1984.
(b)NORAPS mean wind stress for January 1985.
(c)NORAPS mean wind stress for April 1985.
(d)NORAPS mean wind stress for July 1985.

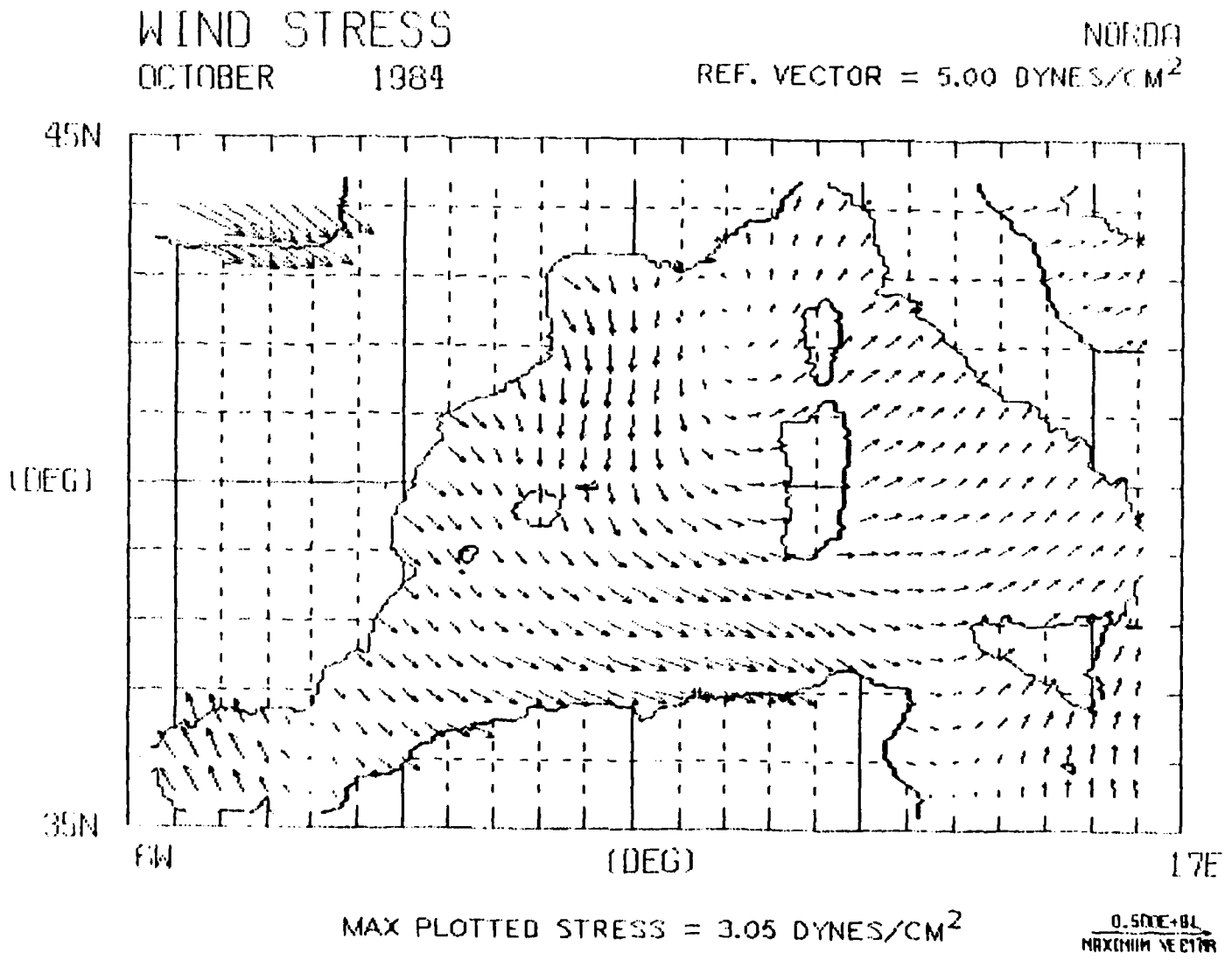
WIND STRESS
OCTOBER 1984
NORDA
REF. VECTOR = 5.00 DYNES/CM^2
45N
(DEG)
35N
80W
(DEG)
17E
MAX PLOTTED STRESS = 3.05 DYNES/CM^2
0.500E+01
MAXIMUM VECTOR

FIGURE 17(a)

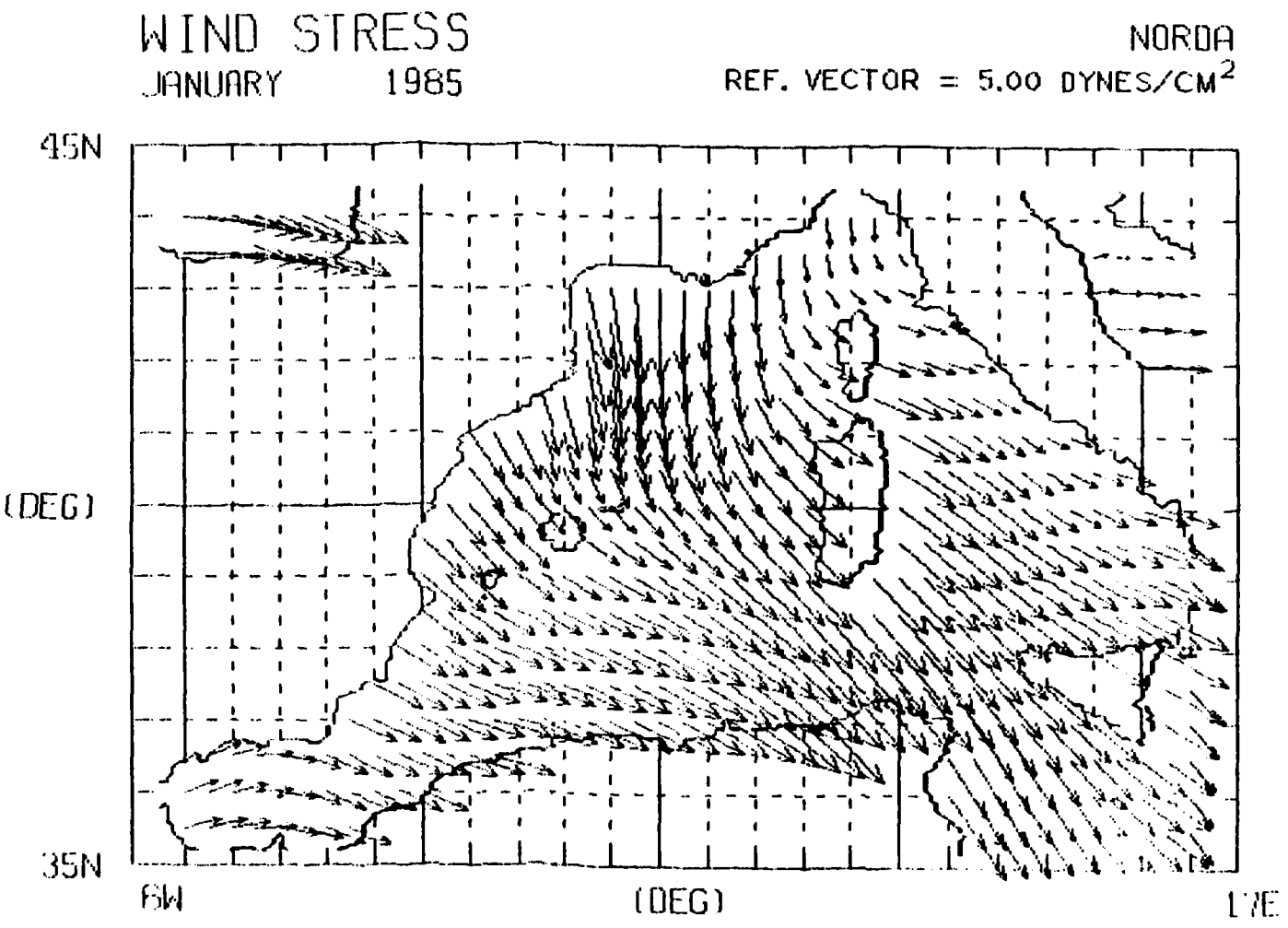
WIND STRESS
JANUARY 1985
NORDA
REF. VECTOR = 5.00 DYNES/CM2
45N
(DEG)
35N
6W
(DEG)
17E
MAX PLOTTED STRESS = 3.83 DYNES/CM2
0.50E+01
MAXIMUM VECTOR

FIGURE 17(b)

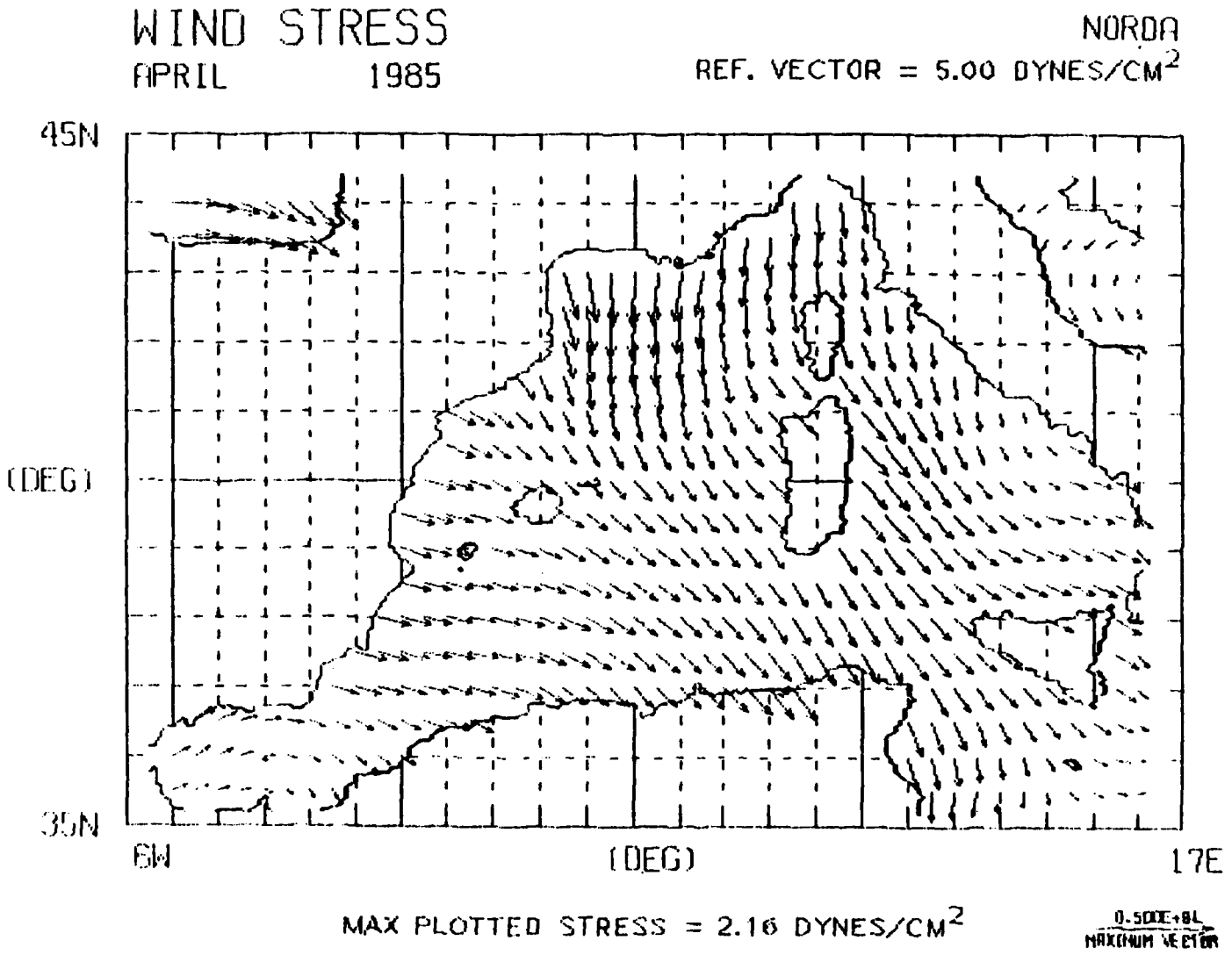
WIND STRESS
APRIL 1985
NORDA
REF. VECTOR = 5.00 DYNES/CM2
45N
(DEG)
35N
6W
(DEG)
17E
MAX PLOTTED STRESS = 2.16 DYNES/CM2
0.500E+01
MAXIMUM VECTOR

FIGURE 17(c)

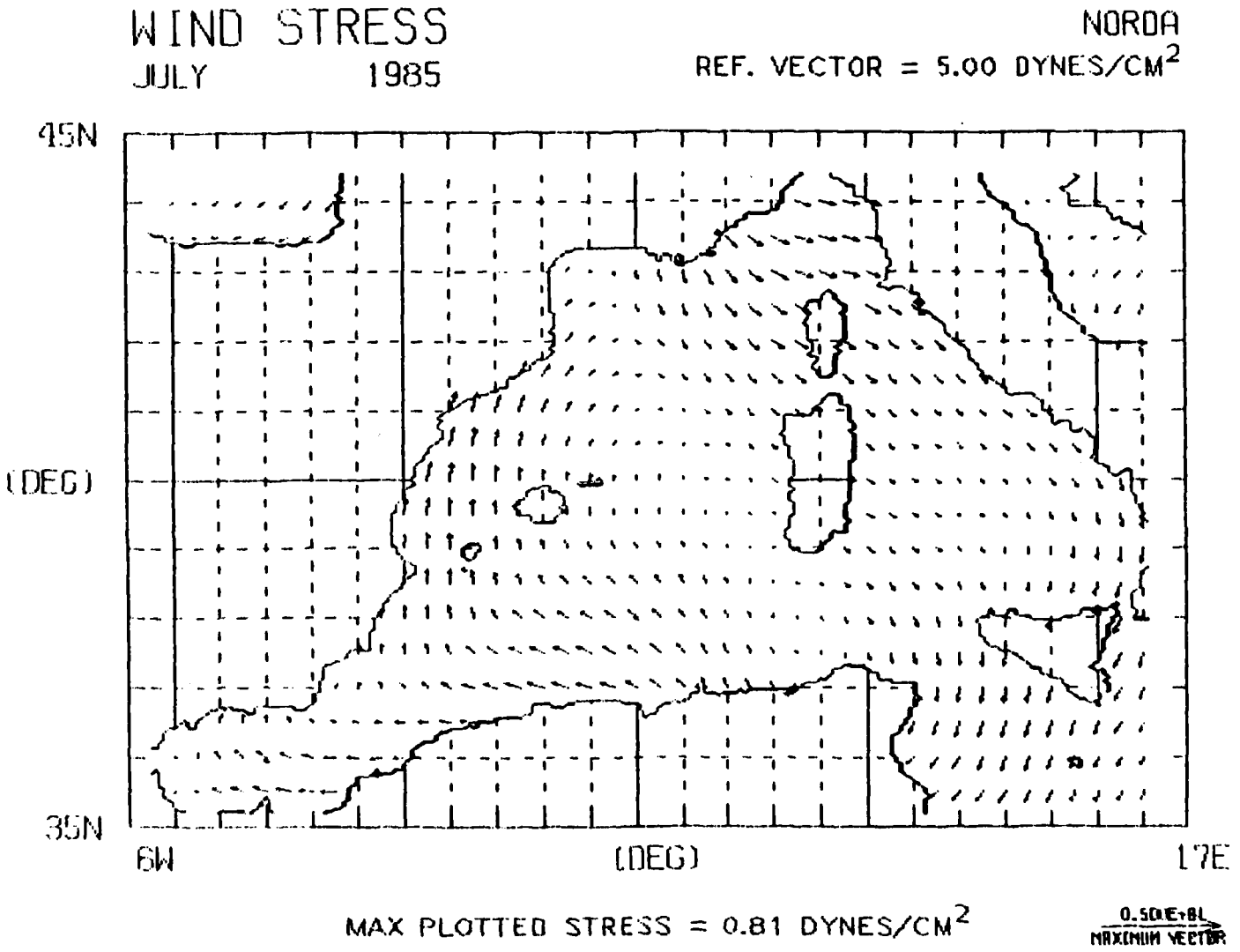
WIND STRESS
JULY 1985
NORDA
REF. VECTOR = 5.00 DYNES/CM2
45N
(DEG)
35N
6W
(DEG)
17E
MAX PLOTTED STRESS = 0.81 DYNES/CM2
0.50E+01
MAXIMUM VECTOR

FIGURE 17(d)

FIGURE 18: (a)NORAPS mean wind stress curl for October 1984.
(b)NORAPS mean wind stress curl for January 1985.
(c)NORAPS mean wind stress curl for April 1985.
(d)NORAPS mean wind stress curl for July 1985.

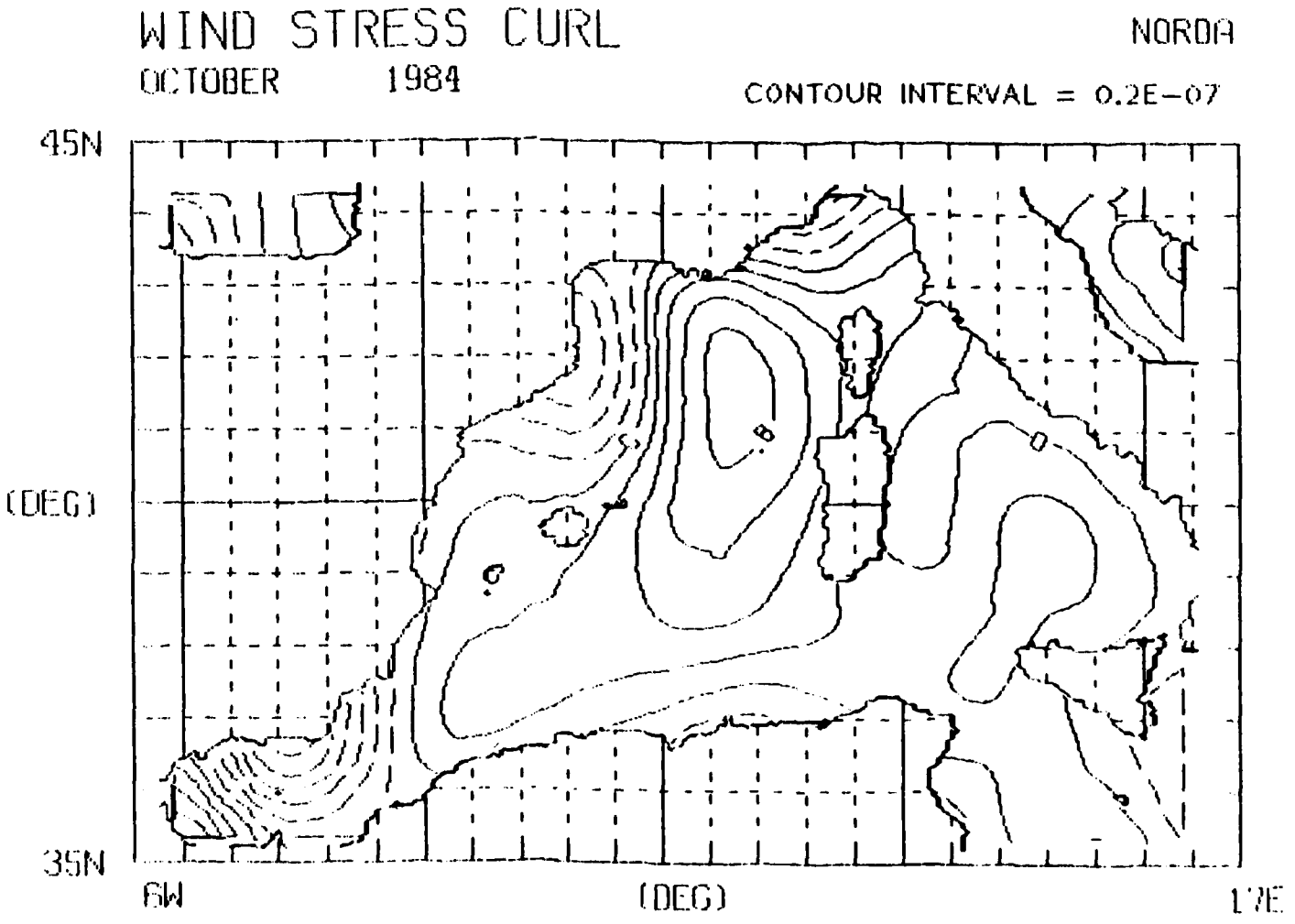
WIND STRESS CURL
NORDA
OCTOBER 1984
CONTOUR INTERVAL = 0.2E-07
45N
(DEG)
35N
6W
(DEG)
17E
RANGE IS -0.1E-06 TO 0.9E-07

FIGURE 18(a)

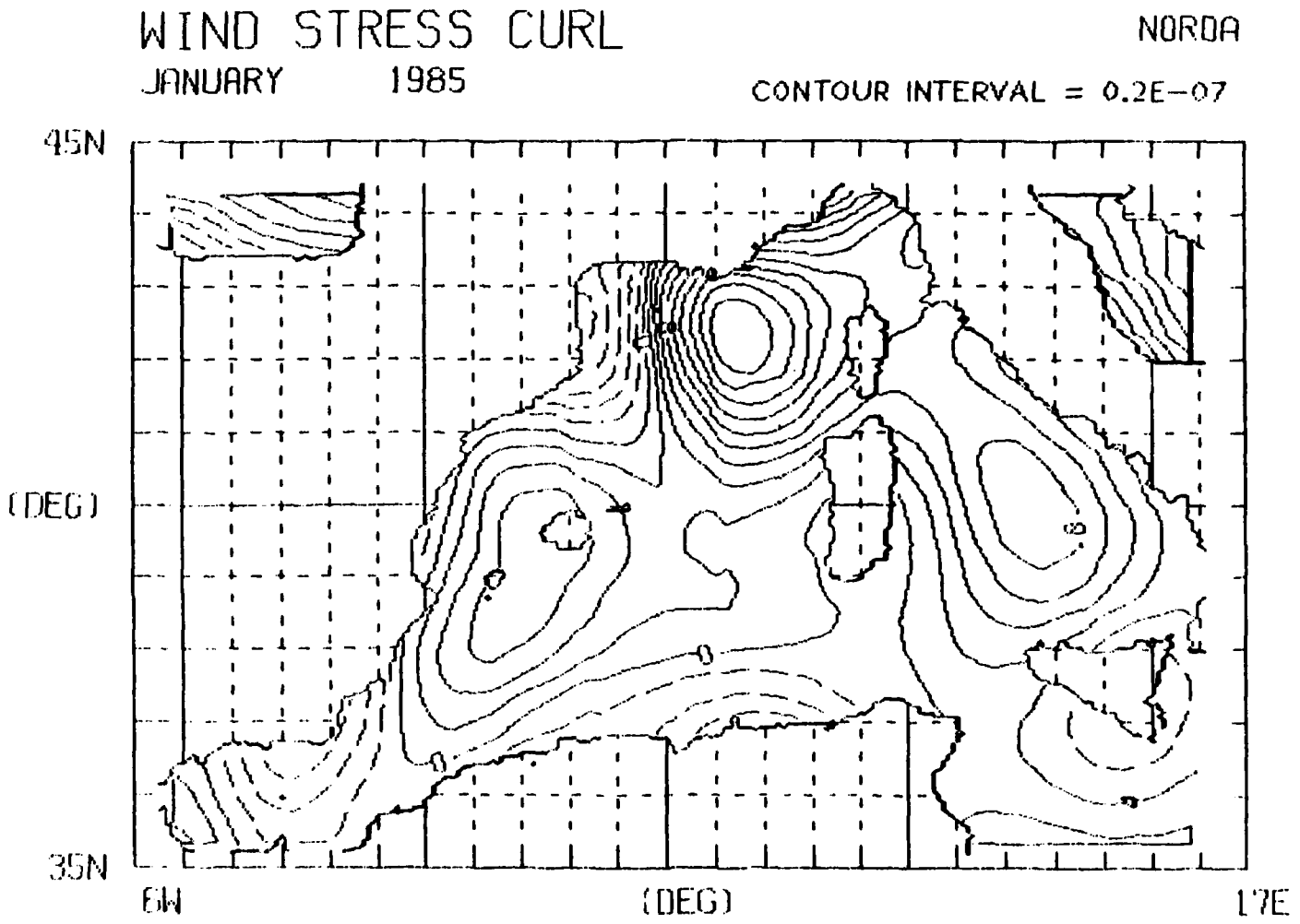
WIND STRESS CURL
NORDA
JANUARY 1985
CONTOUR INTERVAL = 0.2E-07
45N
(DEG)
35N
6W
(DEG)
17E
RANGE IS -0.1E-06 TO 0.2E-06

FIGURE 18(b)

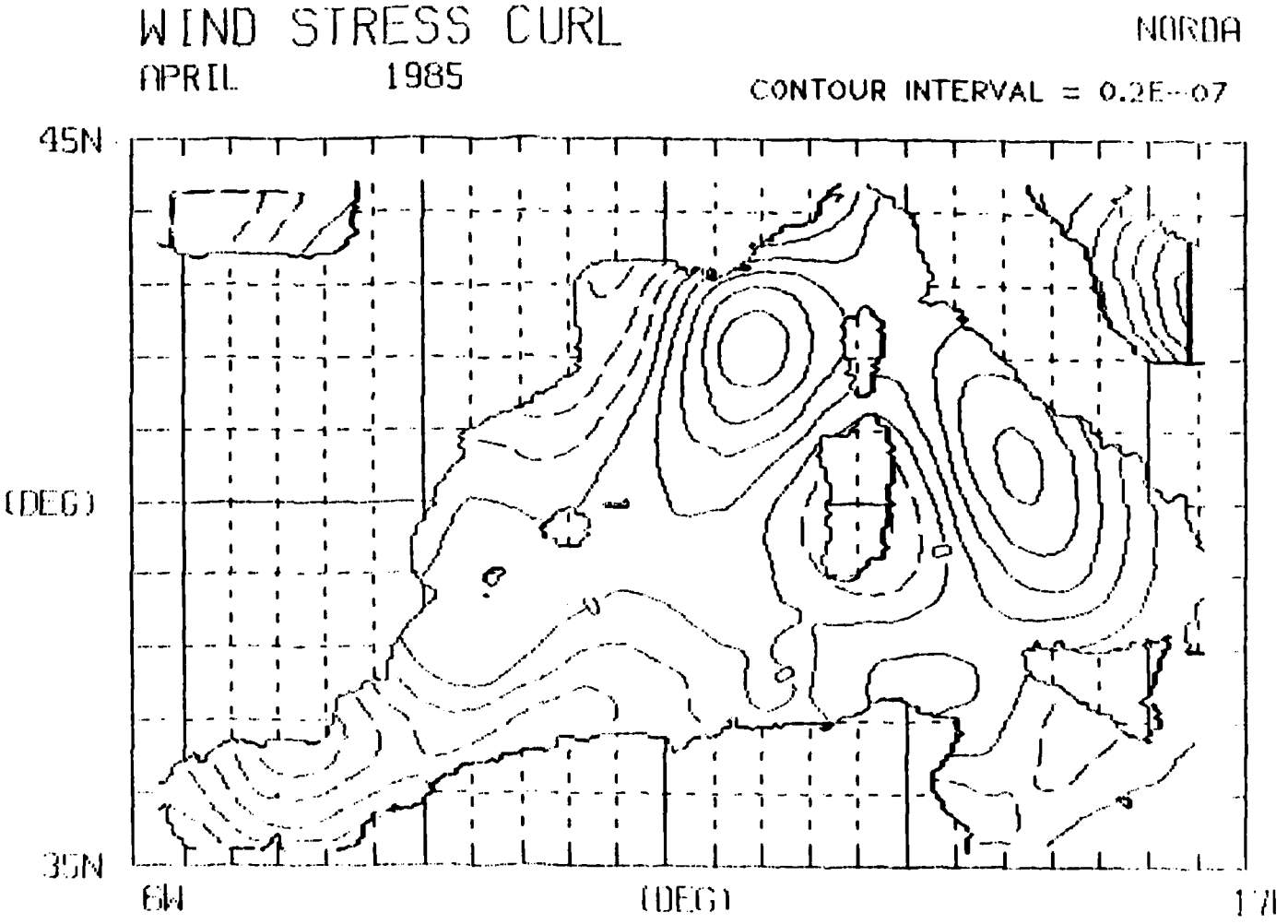
WIND STRESS CURL
NORDA
APRIL 1985
CONTOUR INTERVAL = 0.2E-07
45N
(DEG)
35N
6W
(DEG)
17
RANGE IS -0.1E-06 TO 0.1E-06

FIGURE 18(c)

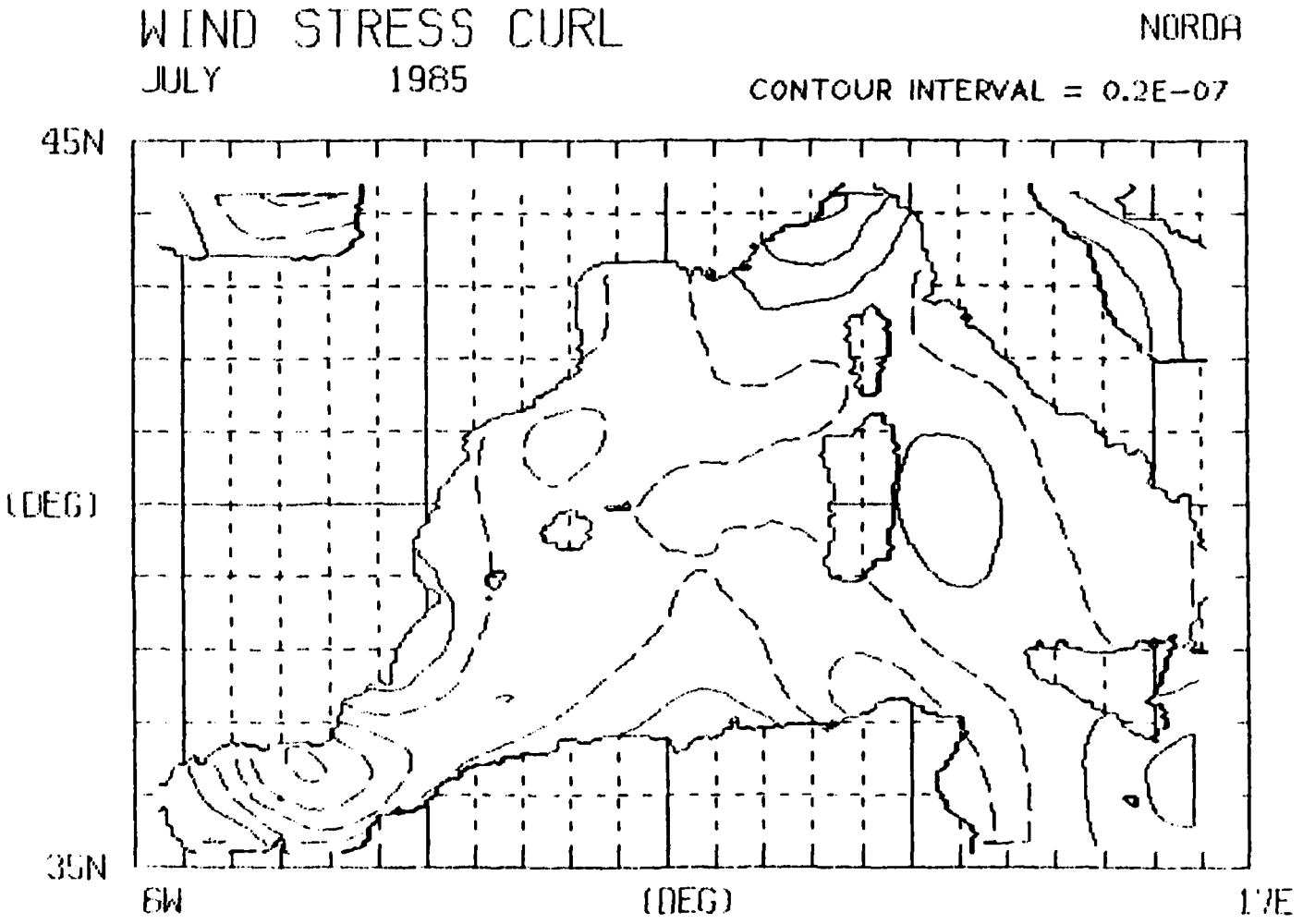

RANGE IS -0.3E-07 TO 0.8E-07

FIGURE 18(d)

FIGURE 19: The "true" (model calculated) lower layer pressure at day 2340, near the middle of the seventh year of experiment E1. The contour interval is 0.08 m^2/s^2.

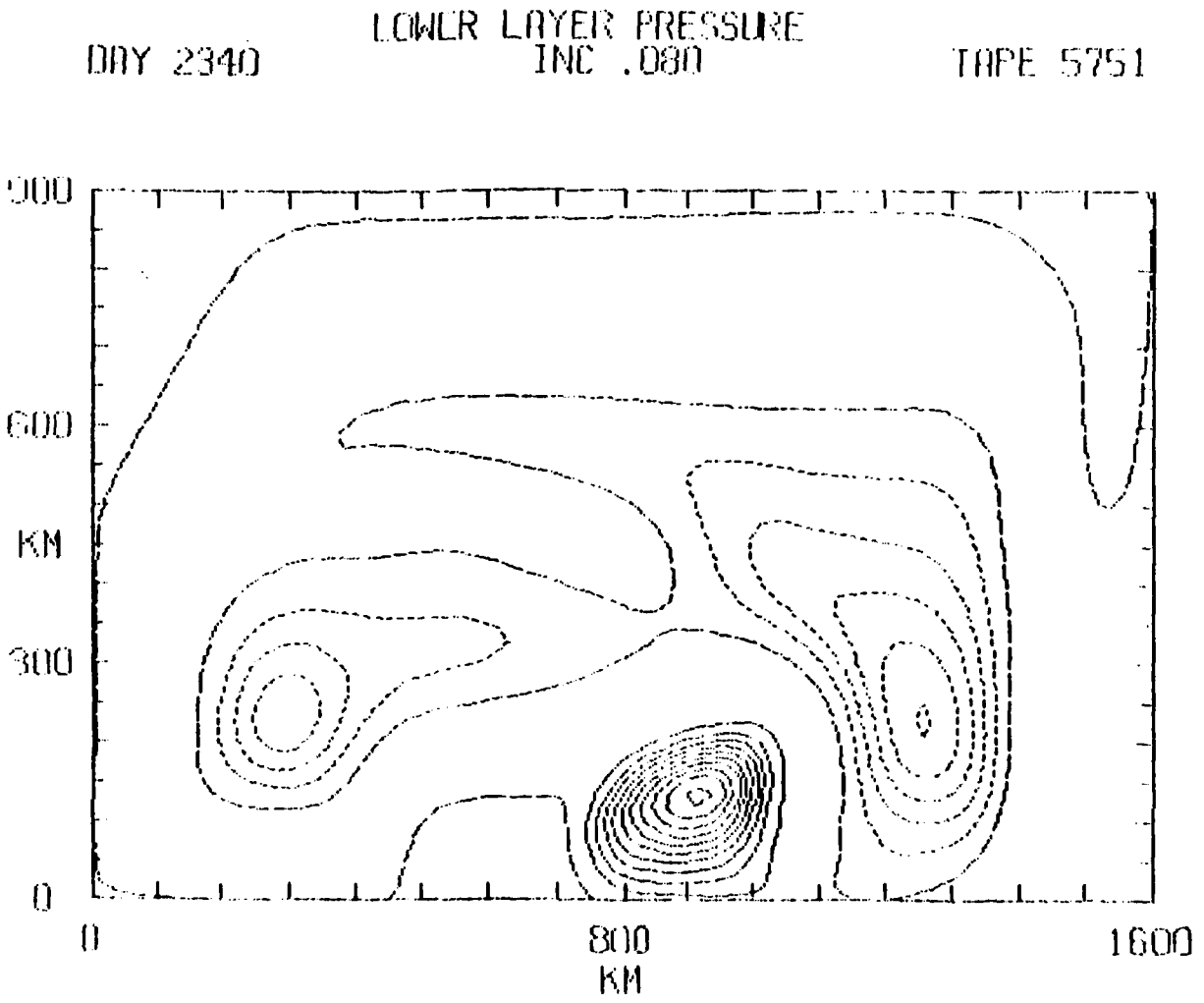
LOWER LAYER PRESSURE
DAY 2340
INC .080
TAPE 5751
900
600
KM
300
0
0
800
1600
KM

FIGURE 19

FIGURE 20: The MPCR predicted lower layer pressure in experiment E1 at day 2340. The contour interval is 0.08 m^2/s^2, and labels are scaled by 1000.

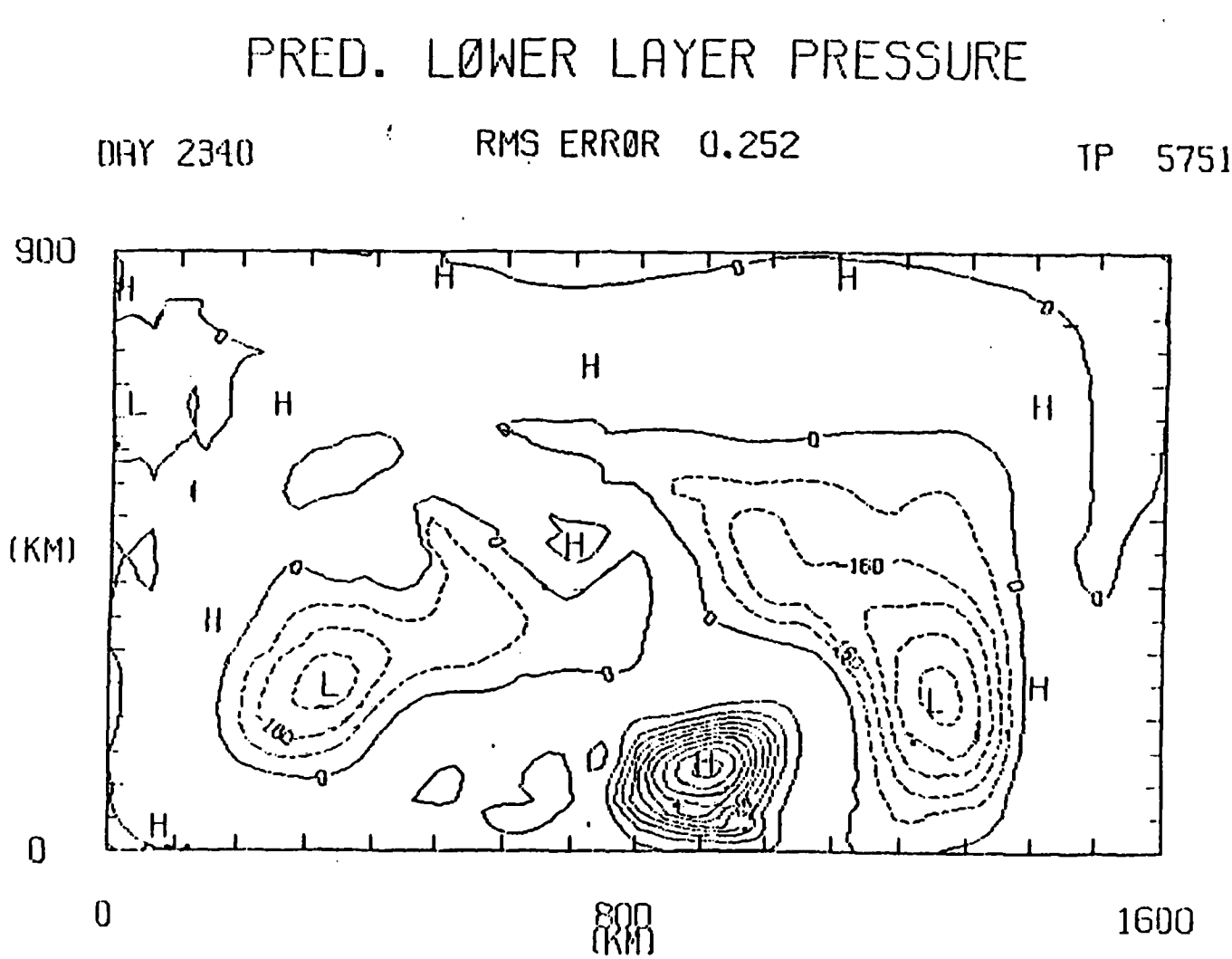
PRED. LØWER LAYER PRESSURE
DAY 2340
RMS ERRØR 0.252
TP 5751
900
(KM)
0
0
800
(KM)
1600
H
L
160
100

FIGURE 20

FIGURE 21: The "true" upper layer pressure on day 1710, near the end of the fifth year of experiment E2. The square box circumscribes a 300 km by 300 km region centered on the major Loop Current eddy. The contour interval is 0.5 m^2/s^2.

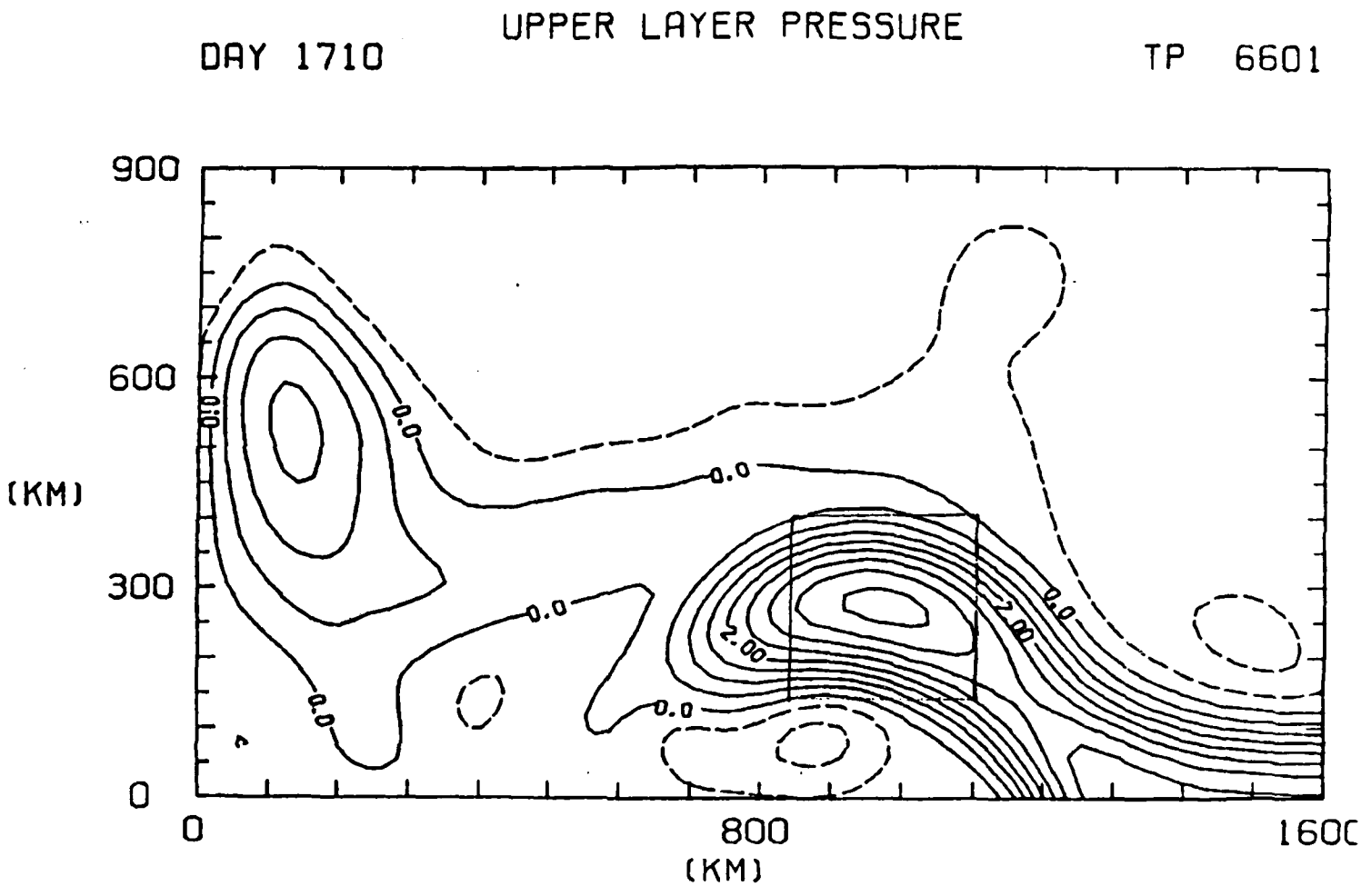
UPPER LAYER PRESSURE
DAY 1710
TP 6601
900
600
300
0
(KM)
0.0
0.0
0.0
0.0
0.0
2.00
2.00
0
800
1600
(KM)

FIGURE 21

FIGURE 22: The "true" lower layer pressure on day 1710 from experiment E2. The contour interval is 0.1 m^2/s^2.

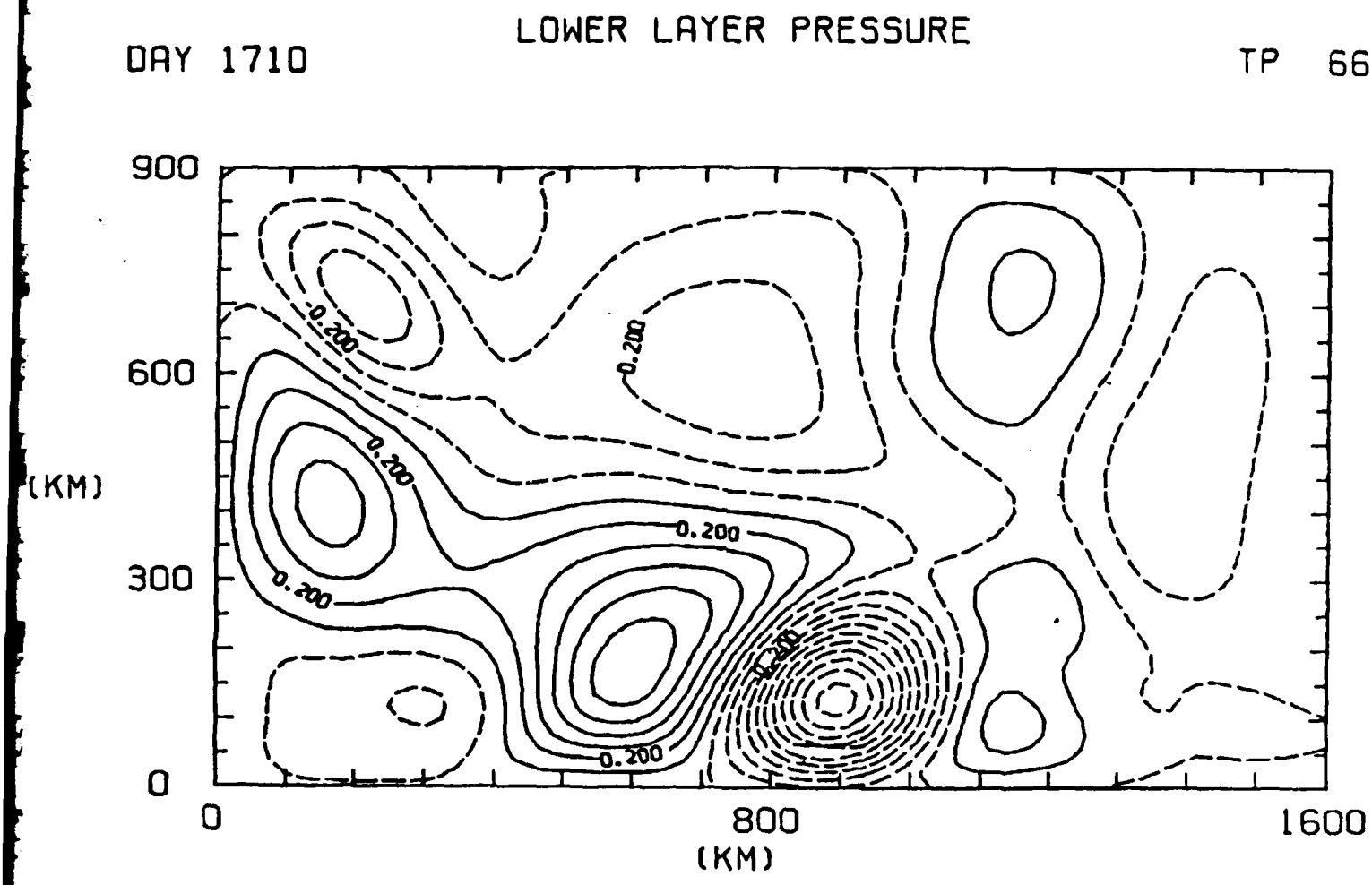
LOWER LAYER PRESSURE
DAY 1710
TP 660
900
600
300
0
(KM)
0
800
1600
(KM)
-0.200
0.200
0.200
0.200
0.200
0.200
-0.200

FIGURE 22

FIGURE 23: MPCR predicted lower layer pressure at day 1710 of experiment E2. The contour interval is 0.1 m^2/s^2.

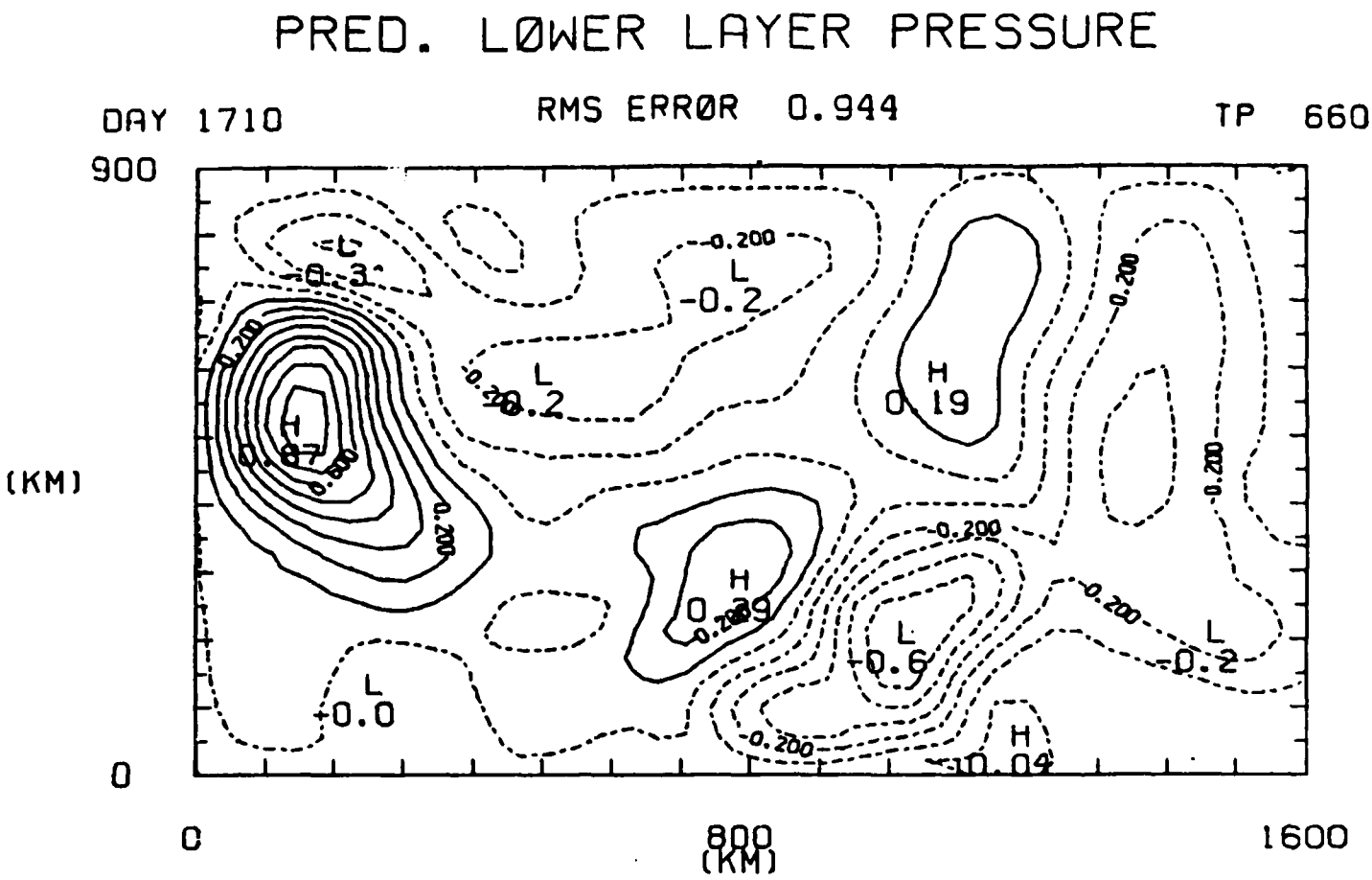

FIGURE 23

CONTOUR FROM -0.80000 TO 0.80000 CONTOUR INTERVAL OF 0.10000E 00 PT(3,3)= -0.14780E-01

FIGURE 24: "Real" lower layer pressure in the region boxed in Figure 21 surrounding the center of the major Loop Current eddy on day 1710 of experiment E2. The contour interval is 0.1 m^2/s^2, and labels are scaled by 100.

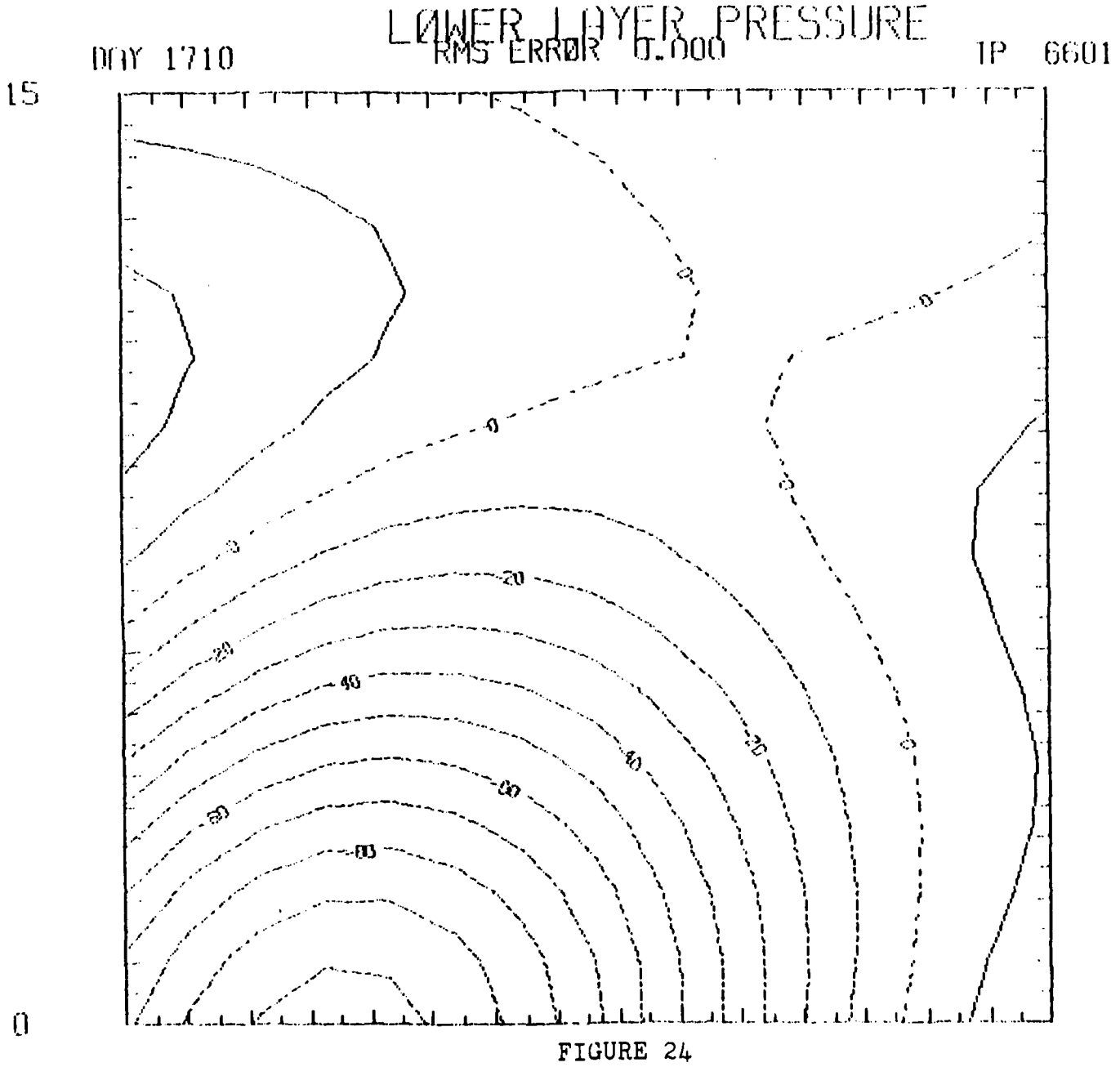

FIGURE 24

CONTOUR LOW 0.00000E-03 TO -0.98800 CONTOUR INTERVAL OF 0.10000 PTS.SI= -0.83163 LABELS SCALED BY 100.00

FIGURE 25: MPCR predicted lower layer pressure for the region shown in Figure 24, also at day 1710. The contour interval is 0.1 m^2/s^2, and labels are scaled by 100.

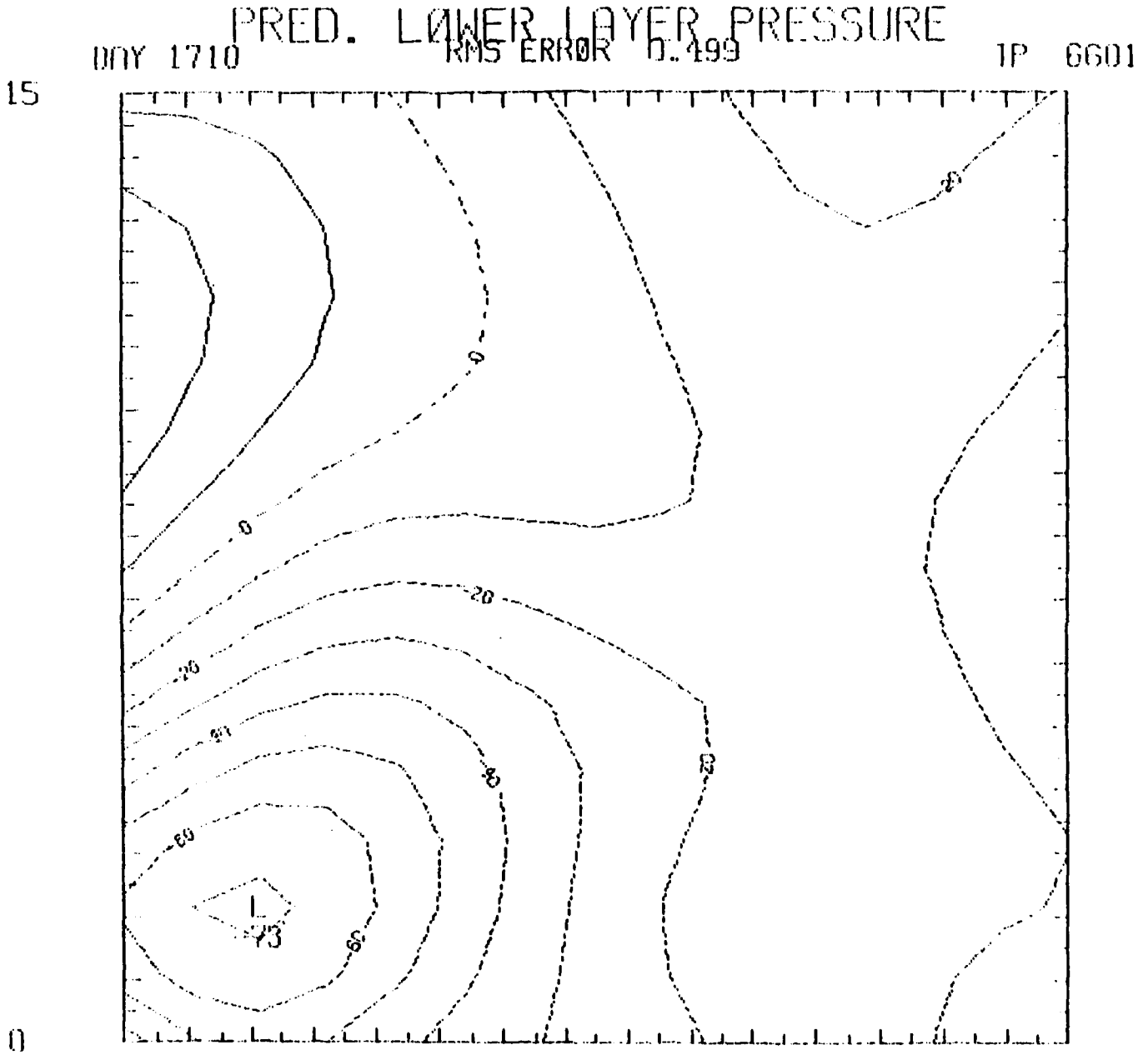

FIGURE 25

CONTOUR FROM 0.30000E-03 TO -0.39000 CONTOUR INTERVAL OF 0.10000 MIN/MAX= -0.72500 LABELS SCALED BY 100.00

END

FILMED

1-86

DTIC